Hamiltonian Cycles on Ammann-Beenker Tilings

Shobhna Singh,[1,*] Jerome Lloyd,[2] and Felix Flicker[3]
[1]*School of Physics and Astronomy, Cardiff University, The Parade, Cardiff CF24 3AA, United Kingdom*
[2]*Department of Theoretical Physics, University of Geneva, 24 rue du Général-Dufour, 1211 Genève 4, Switzerland*
[3]*School of Physics, Tyndall Avenue, Bristol BS8 1TL, United Kingdom*

(Received 13 March 2023; revised 25 January 2024; accepted 1 May 2024; published 10 July 2024)

We provide a simple algorithm for constructing Hamiltonian graph cycles (visiting every vertex exactly once) on a set of arbitrarily large finite subgraphs of aperiodic two-dimensional Ammann-Beenker (AB) tilings. Using this result, and the discrete scale symmetry of AB tilings, we find exact solutions to a range of other problems which lie in the complexity class NP-complete for general graphs. These include the equal-weight traveling salesperson problem, providing, for example, the most efficient route a scanning tunneling microscope tip could take to image the atoms of physical quasicrystals with AB symmetries; the longest path problem, whose solution demonstrates that collections of flexible molecules of any length can adsorb onto AB quasicrystal surfaces at density one, with possible applications to catalysis; and the three-coloring problem, giving ground states for the q-state Potts model ($q \geq 3$) of magnetic interactions defined on the planar dual to AB, which may provide useful models for protein folding.

DOI: 10.1103/PhysRevX.14.031005

Subject Areas: Condensed Matter Physics, Statistical Physics

I. INTRODUCTION

Fractal geometric loop structures are ubiquitous in physics, appearing often as the natural degrees of freedom in models of critical phenomena. Examples include the fluctuating domain walls of an Ising magnet, the compact shapes of long polymer chains [1], or the space-time trajectories of quantum particles. A special class of loops, attracting much attention beyond physics, are the Hamiltonian cycles. A Hamiltonian cycle of a graph is a closed, self-avoiding loop that visits every vertex precisely once. Study of these objects dates at least to the ninth century A.D., when the Indian poet Rudrata constructed a poem based on a "knight's tour" of the chessboard. Since then they have appeared in a variety of applications in the sciences and mathematics including protein folding [2,3], traffic models, spin models in statistical mechanics [4,5], and ice-type models of geometrically frustrated magnetism [6,7].

Hamiltonian cycles have been used to model the statistics of polymer melts [1,8–10]: For example, the critical scaling exponents were calculated for polymer chains in 2D using the self-avoiding walk on the honeycomb lattice [11,12]. They have also played a key role in the study of protein folding [1,2,13–16]. The shapes ("conformational properties") of proteins play a significant role in their biological function. Proteins often adopt remarkably compact and symmetrical structures compared to the more general class of polymers [14]. A key question is how to predict 3D conformational properties from the 1D sequences of amino acids from which the proteins are built. One route is to study "simple exact models" in which the amino acids are represented by structureless units, each occupying the vertex of a graph. Neighboring units in the protein must be nearest neighbors on the graph. The graphs are chosen to have specific geometrical embeddings, typically periodic lattices. While not providing accurate geometrical models, such approaches have the advantage of being exactly solvable. They are also able to capture "nonlocal" interactions, in which amino acids interact when they are neighbors on the graph but not on the 1D chain itself [1,9,13,17,18]. Remarkably, 2D graphs often give qualitatively similar results to 3D graphs while affording a significant computational advantage [14]. Simple exact models have also been instrumental in the development of polymer physics more generally [8,19–22].

The $O(n)$ model in statistical physics, which describes n-component spins interacting with their nearest lattice neighbors with isotropic couplings [4,5], can be mapped to a problem involving self-avoiding loops [17,23]. The probability of a given loop configuration is weighted according to two fugacities: x weighting the total perimeter of the loops, and n the number of loops. The $O(n)$ phase

*shobhna862@gmail.com

diagram encapsulates many well-known models in statistical physics. For example, the ferromagnetic Ising model arises for $n = 1$, where the loops represent the domain walls in the low temperature limit (thus the Ising spins are defined on the planar dual lattice), while in the high temperature limit the natural degrees of freedom are again loops, though their expression in terms of the original spin variables is less intuitive. The q-state Potts models can be related to the $n = \sqrt{q}$ limit. As $x \to \infty$ every lattice site is visited by a loop and one arrives at the so-called "fully packed loop" (FPL) models, which additionally model crystal surface growth. In the $x \to \infty, n \to 0$ limit, the system is forced into a single macroscopic loop traversing every site of the system, which is a Hamiltonian cycle [23,24]. Studying Hamiltonian cycles can thus lead to an understanding of a variety of other models in a given system, and for this reason a great deal of work has been put into their study—primarily in the simplest context of periodic regular lattices [5,9,11,17,18,24–37]. Given, however, that the complex fractal structures (e.g., polymer-protein structures) these objects aim to model often lack translational symmetry and favor disordered growth [38], studies of Hamiltonian cycles in settings where translational symmetry is absent may unearth important clues toward the universality of these results.

In this paper we present a simple algorithm for constructing Hamiltonian cycles and fully packed loops on a set of arbitrarily large finite subgraphs of infinite graphs which do not admit periodic planar embeddings. Specifically, we consider graphs formed from subsets of the edges and vertices of Ammann-Beenker (AB) tilings (Fig. 1). These are two-dimensional (2D) infinite aperiodic tilings [39–41] built from two tiles, a square and a rhombus. They lack the translational symmetry of periodic lattices but nevertheless feature long-range order, evidenced by sharp spots in their diffraction patterns [40,42,43]. The long-range order of AB enables exact analytical results to be proven, while their infinite extent allows consideration of the thermodynamic limit of an infinite number of vertices, of interest in condensed matter physics where physical quasicrystals are known with the symmetries of AB [44,45]. Recent experiments have demonstrated tunable quasicrystal geometries in

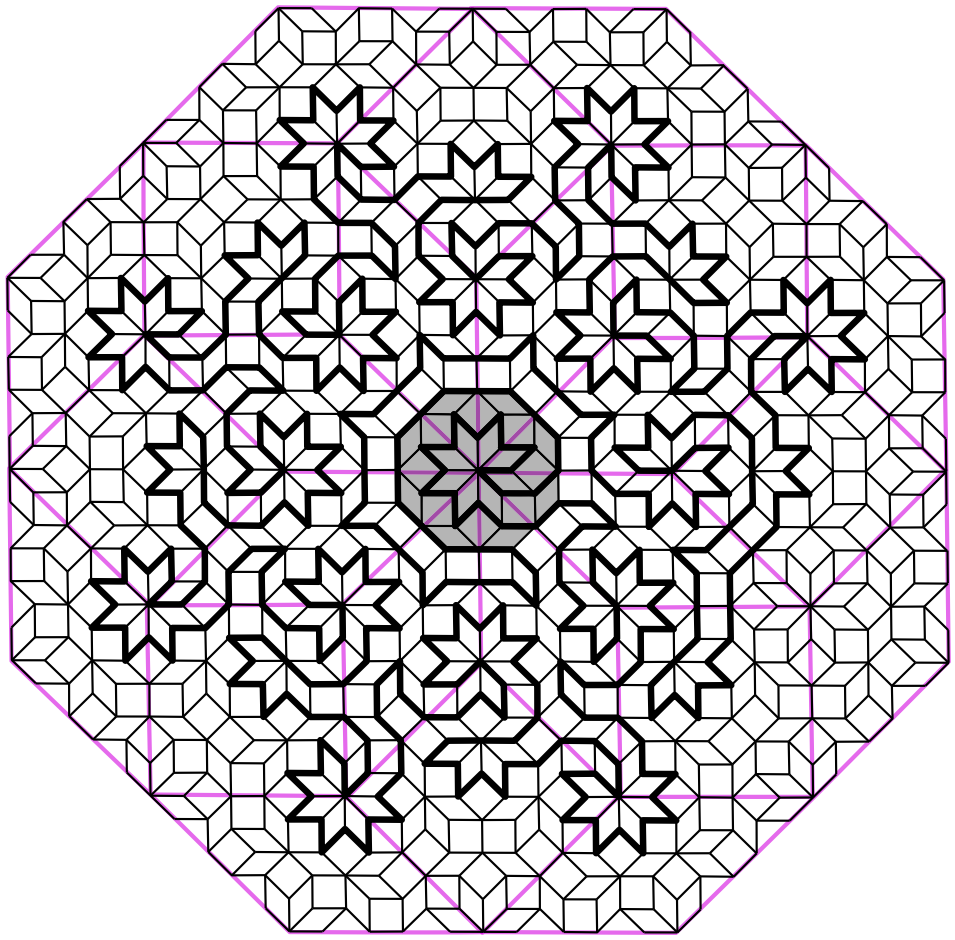

FIG. 1. A patch of AB tiling showing the eightfold symmetric region W_1, and W_0 in gray. W_1 is the twice inflation of W_0, formed from the double-inflated tiles shown in Fig. 2; purple lines show the boundary of these tiles (and do not belong to the tiling itself). The thick black edges form a Hamiltonian cycle on the set of vertices they visit; this set is termed U_1.

twisted trilayer graphene [46], while eightfold symmetric structures have also been created in optical lattices [47,48]. Quasicrystals host a broad range of exciting physical phenomena from exotic criticality [49–51] to charge order [52,53] to topology [53–55], with the lack of periodicity often leading to novel behaviors.

Efficient Hamiltonian cycle constructions exist for certain special classes of graph [56–58]. One example is four-connected planar graphs, defined as requiring the deletion of at least four vertices to disconnect them [59]. This result was recently employed in the elegant design of "quasicrystal kirigami" [60] using a construction based on Hamiltonian cycles defined on the planar dual to AB. However, to our knowledge AB tilings themselves are not covered by any such special case (they are three-connected). The unexpectedness of (arbitrarily large finite subgraphs of) AB tilings' admittance of Hamiltonian cycles can be seen by comparison to rhombic Penrose tilings, which are in many ways similar to AB. These, too, are a set of infinite 2D tilings built from two tile types (two shapes of rhombus); they are again aperiodic but long-range ordered, and the resulting graphs are bipartite, meaning the vertices divide into two sets such that vertices in one set connect only to vertices in the other—another property shared with AB. Yet Penrose tilings cannot admit Hamiltonian cycles, because they do not admit perfect dimer matchings (sets of edges such that each vertex meets precisely one edge) [61]. The latter is a necessary condition for the former, since deleting every second edge along a Hamiltonian cycle results in a perfect matching. It is difficult to think of any special case which could cover AB tilings which would not also cover Penrose tilings.

The difficulty of constructing Hamiltonian cycles in arbitrary graphs can be made precise using the notion of computational complexity. Given a graph, the question of whether it admits a Hamiltonian cycle lies in the complexity class "nondeterministic polynomial time complete" (NPC) [62,63]. These problems are prohibitively hard to solve—the fastest known exact algorithms scale exponentially—but a given solution can be checked quickly, in polynomial time (P). Completeness refers to the fact that if a polynomial-time algorithm were found which solved any NPC problem, all problems in the broader class NP would similarly simplify. Loosely, all problems in NP contain a bottleneck in NPC.

We do not purport to solve an NPC problem. Rather, we show that AB is a previously unknown special case of the Hamiltonian cycle problem which lies in P rather than NPC. As such, it does not follow that all NP problems can be solved in polynomial time on AB. However, we might reasonably hope that our Hamiltonian cycles permit new solutions to certain problems on AB, and indeed we find that this is the case. Using both the Hamiltonian cycles and the inherited discrete scale symmetry of AB tilings, we find exact solutions on AB to a range of other nontrivial problems which are NPC in general graphs [63]. We present three cases which have important applications to physics.

For example, by solving the equal-weight traveling salesperson problem (Sec. IV A) on AB we provide a maximally efficient route for a scanning tunneling microscopy (STM) tip to follow in order to scan every atom on the surface of an AB quasicrystal in a given area. Given that a state-of-the-art STM measurement might take on the order of a month, such efficient routes are highly desirable. The problem of finding them is not present in periodic crystals, where efficient routes can be found by following crystal symmetries.

By solving the longest path problem (Sec. IV B) on AB we identify the longest possible path visiting every site within a given region. This shows that long, flexible molecules, such as polymers, can adsorb onto the surface of AB quasicrystals with maximal efficiency. Moreover, by breaking the longest path into smaller units, our solution demonstrates that collections of flexible molecules of arbitrary lengths can also adsorb at maximal packing density. This has potential applications to catalysis, in which the activation energy of a reaction between molecules is lowered by having them adsorb onto a surface. Quasicrystal surfaces are emerging as an interesting material for adsorption because they provide different local environments with a range of bond angles [64], in contrast to the periodic surfaces of crystals. They have potential applications in hydrogen adsorption and storage [65,66], low friction machine parts, and nonstick coatings [65,67].

The three-coloring problem asks whether it is possible to color the tiles of a planar tiling with three colors such that no two tiles sharing an edge share a color [68]. We solve this problem on AB in Sec. IV C. The three colors can represent the degrees of freedom in the three-state Potts model of nearest-neighbor magnetic interactions. The three-colored AB tiling thereby gives an unfrustrated ground state for the antiferromagnetic q-state Potts model, with spins defined on the faces of AB, for any $q \geq 3$.

The Potts model was originally introduced to describe interactions between magnetic ions [68,69], gaining relevance to quasicrystals with the discovery of ordered magnetic states in these materials [70–74]. More recently it, too, has been used as a simple model of protein folding, with Potts variables representing the q species of amino acid comprising the protein chain [3,75,76]. The interaction between amino acids can be either repulsive or attractive depending on the solvent which surrounds the protein. Compared to the typical approximation that the protein folds on a square lattice [1,9,76], AB arguably defines a better approximation to the real problem, in which the amino acids have continuous spatial degrees of freedom. This is because AB has a larger range of bond angles, better approximating a continuous rotational symmetry than any 2D regular lattice.

In Appendix B we solve a further three problems, on AB, which are known to be NPC in general graphs: the minimum dominating set problem (Sec. B 1), the domatic number problem (Sec. B 2), and the induced path problem (Sec. B 3). Doubtless many more examples can be found. The fact that many NPC problems admit polynomial-time solutions on AB suggests that the discrete scale symmetry of quasiperiodic lattices may be as powerful a simplifying factor as the discrete translational symmetry widely used to obtain exact results on periodic lattices.

The remainder of this paper is organized as follows. We introduce the necessary background on the AB tilings and graph theory in Sec. II. In Sec. III we prove the existence of Hamiltonian cycles on arbitrarily large finite subgraphs of AB tilings. We prove along the way the possibility of fully packed loops, and give details of our algorithm. In Sec. IV we utilize the approach to present exact solutions, on the same graphs, to three problems which are NPC for general graphs: the equal-weight traveling salesperson problem (Sec. IV A), the longest path problem (Sec. IV B), and the three-coloring problem (Sec. IV C). We comment on the applications for each. In Appendix B we provide exact solutions to three other problems on these graphs: the minimum dominating set problem (Appendix B 1), the domatic number problem (Appendix B 2). and the induced path problem (Appendix B 3). In Sec. V we place these results in a broader context.

II. BACKGROUND

A. Ammann-Beenker tilings

The quasicrystal stuctures represented by the Ammann-Beenker tilings lack the translation symmetry of periodic graphs and, accordingly, mathematical results in the thermodynamic limit are more challenging to obtain. However, the translation symmetry of ordinary crystals is replaced by a *discrete scale symmetry* which underlies the unique features of quasicrystal systems.

We will first describe the construction of the AB tilings in the thermodynamic limit [77], and then discuss the scale symmetry of the tilings, which is central to our proof of Hamiltonian cycles.

Each tiling is built from two basic building blocks, called prototiles: a square tile and a rhombic tile with acute angle $\pi/4$. Both tiles are taken to have unit edge length. Starting from any "legal" patch of a few tiles [78], the tiling is then built by repeatedly applying an "inflation rule" to the tiles: Every tile is first "decomposed" into smaller copies of the two tiles, as defined in Fig. 2, and then the new edges are rescaled (inflated) by a factor of the silver ratio, $\delta_S = 1 + \sqrt{2}$, so that the tiles have unit edge length again. The edges and vertices of the tiling define a graph. The graph is bipartite, meaning the vertices divide into two subsets where edges of the graph only join members of one subset to the other. Since the arguments presented in this paper rely only on the connectivity of the graph, the rescaling is not important for our purposes—hence, inflation and decomposition are interchangeable in what follows. Under inflation, the number of tiles grows exponentially and the infinite tiling is recovered in the limit

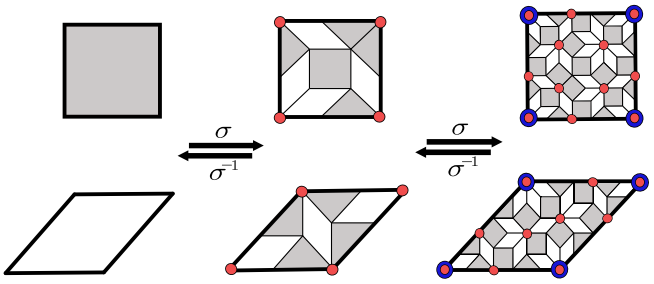

FIG. 2. The "inflation" rule σ, in which a tile is decomposed into smaller tiles. Typically this would be followed by a rescaling (inflation) of all lengths by a factor of the silver ratio $\delta_S = 1 + \sqrt{2}$, although as we are only concerned with graph connectivity, inflation and decomposition are equivalent. Vertices of once- and twice-inflated tiles are shown in red and blue, respectively. We denote the once-inflated tiles to be level $L_{1/2}$ and the twice-inflated tiles to be level L_1.

$$\mathcal{T} = \lim_{n\to\infty} \sigma^n(\mathcal{T}_0), \tag{1}$$

where $\mathcal{T}$ is the infinite tiling, σ the inflation rule, and $\mathcal{T}_0$ the initial patch. We use "tiling" to mean the infinite tiling, and "patch" when referring to any finite set of connected tiles. The inverse process, termed "deflation," equivalently "composition" (followed by a rescaling), is uniquely defined and follows from the inflation rules.

The set of Ammann-Beenker tilings that can be created by inflation has infinite cardinality. There are two important consequences that follow from the inflation structure [77] which will be important later.

First, we take graph edges to be of unit length.

Definition II.1 (Linear repetitivity [77,79]). There is a finite $C > 0$ such that, for any set of vertices V appearing within a disk of radius r, every disk of radius Cr contains a copy of V.

AB is linearly repetitive [77].

Definition II.2 (Local isomorphism [40]). Two tilings are locally isomorphic if any finite patch appearing in one appears in the other.

All AB tilings are locally isomorphic to one another [40,77]. In this paper AB refers to the set of all AB tilings unless otherwise stated. As a result of linear repetitivity and local isomorphism, it should be understood that reference to a vertex set V in a particular AB tiling is meant modulo translations.

Within the locally isomorphic set we will not differentiate between arbitrary rescalings of the tilings. As the simplest example of this isomorphism, the set of edges and tiles surrounding each vertex in the tiling belongs to one of

seven unique configurations, which we call "m-vertices" (where m labels the vertex connectivity). In total the vertex configurations for AB are given by the 3-, 4-, 5_A-, 5_B-, 6-, 7- and 8-vertices, with each configuration appearing with a frequency given by a function of the silver ratio δ_S. The 3-vertex, for example, occurs most frequently and makes up a fraction $\delta_S - 2$ (∼40%) of the AB vertices. The two configurations with five edges are distinguished by their behavior under inflation.

A special role is played by the 8-vertices of the tiling, as every vertex configuration inflates to an 8-vertex under at most two inflations [39]. This means that edges can be drawn between 8-vertices of an AB tiling so as to generate another AB tiling. Figure 1 highlights this symmetry. Similarly, some of the 8-vertices of the original tiling sit also at 8-vertices of the composed tiling, and therefore logically form the *four-times* composed tiling. This hierarchy continues and results in the discrete scale symmetry exhibited by the AB tiling and several other aperiodic tilings, in turn responsible for many of the remarkable physical properties of quasicrystals.

We call an 8-vertex an 8_0-vertex if under twice deflation it becomes any m-vertex with $m \neq 8$ (most 8-vertices of the AB tiling are of this type); similarly we call it an 8_1-vertex if it becomes an 8_0-vertex under twice deflation. Generalizing, an 8_n-vertex becomes an 8_0-vertex after $2n$ deflations. The *local empire* of a vertex configuration is the simply connected set of tiles that always appears around the vertex configuration wherever it appears in the tiling [80]. The local empire of the 8_0-vertex, which we call W_0, is shown in Fig. 1 (also shown is the 8_1 empire, W_1): It has a discrete eightfold rotational symmetry (D_8 in Schönflies notation). The inflation rule maps 8_n-vertices to 8_{n+1}-vertices (applying the rule twice) while simultaneously growing the size of the vertex's local empire. The D_8 symmetry is preserved under inflation. Therefore 8_n-vertices are accompanied by D_8-symmetric local empires W_n having a radius of symmetry growing approximately as $R_n \sim \delta_S^{2n}$. Furthermore, the W_n empire contains all $W_{0\leq m\leq n}$ empires.

It follows from linear repetitivity that any finite set of tiles (or vertices) in AB is contained in W_n for sufficiently large n. On account of this, we will often focus on the W_n to prove more general results. It will also prove useful to define a modified version of the AB tiling with all 8-vertices removed, dubbed the AB* tiling [39].

In Fig. 2 we denote the individual square and rhombus (left) to be level L_0 and the *twice* inflated square and rhombus (right) to be level L_1; this is because any vertex inflates to an 8-vertex under two inflations but not one, and the convention follows Ref. [39]. We therefore designate the once-inflated tiles (middle) to be at level $L_{1/2}$.

B. Graph terminology and conventions

A graph $G(V, E)$ is a set of vertices V connected by a set of edges E. We consider undirected graphs, in which no distinction is drawn between the two directions of traversal of an edge. We also consider only bipartite graphs, in which the vertices divide into two sets such that edges only connect one set to the other. The cardinality of a graph is the cardinality of the set of vertices it contains (i.e., the number of vertices in the graph). We denote this $|G|$ [81–83].

We define a path to be a set of edges joining a sequence of distinct vertices, and the length of the path to be the number of edges it contains. Given a set of edges $E' \subset G$ it may be possible to find an "alternating path," which is a path in G along which every second edge belongs to E' but all others do not [81]. We borrow this terminology from the theory of dimer matchings, in which E' is a set of edges such that no two edges share a common vertex, although we consider different structures for E' here. An "augmenting path" is an alternating path in which the first and last edges are not in E'. In general, augmenting an alternating path means to switch which edges along the path are in the set E' and which are not.

In this paper, we consider graphs made from the vertices and edges of Ammann-Beenker tilings. We will use the shorthand $G = \mathrm{AB}$ to denote the case that G is the graph formed from any infinite Ammann-Beenker tiling. We will sometimes refer to graphs formed from finite patches of AB, which should be clear from the context.

III. CONSTRUCTIVE PROOF OF HAMILTONIAN CYCLES

In this section we prove the following.

Theorem 1. Given an AB tiling and a finite set of vertices $V \subset \mathrm{AB}$ there exists a set U_n, where $V \subseteq U_n \subset \mathrm{AB}$, such that U_n contains a Hamiltonian cycle $\mathcal{H}$.

Proof. In Sec. III A we identify a set of edges on the twice-inflated AB tiles such that every $8_{n<0}$ vertex (that is, every vertex which is not an 8-vertex) meets two such edges. This constitutes a set of fully packed loops, visiting every vertex precisely once, on AB*. We then focus on finite tile sets generated by n twice inflations of the local empire of the 8_0-vertex, denoted W_n. These regions have D_8 symmetry. Any finite set of vertices $V \subset \mathrm{AB}$ lies within an infinite hierarchy of W_n for sufficiently large n, as shown in Sec. II. In Sec. III B we identify a method of reconnecting these fully packed loops so as to include into the loops all 8_0-vertices within W_n, and then all $8_{0<m<n}$ vertices where the 8_{m-1} vertices have already been included. The result is fully packed loops on all vertices within W_n except the central 8_n vertex. Finally, we show that a subset of these loops can be joined into a single loop which additionally visits the central vertex. We denote the set of vertices visited by this loop U_n. As the patches U_n grow exponentially with n so as to cover arbitrarily large areas of AB, it follows from linear repetitivity (Definition II.1) that $V \in U_n$ for sufficiently large n.

Since the cycle constructed on U_n visits each of its vertices precisely once, this proves Theorem 1. ∎

The proof is constructive, returning $\mathcal{H}$ given V, and is linear in the number of vertices in U_n. We place a precise bound on the necessary size of U_n for any given V in Sec. III C. Furthermore, the Hamiltonian cycle on U_n visits a simply connected set of vertices whose cardinality increases exponentially with n, and which therefore admits a straightforward approach to the thermodynamic limit. We consider this limit, $U_{n\to\infty}$ in Sec. III D.

A. Constructing fully packed loops on AB*

In Fig. 3 we show the twice inflations of the two prototiles. We denote the smaller tiles as constituting composition level zero L_0, and the larger tiles L_1. We work exclusively with twice inflations, rather than single inflations, as every vertex becomes an 8-vertex under twice inflation, but some do not do so under a single inflation.

In Fig. 3 we highlight (thick black edges) a subset of L_0 edges on each L_1 tile. When the L_1 tiles join into legitimate AB patches, every vertex in L_0 is visited by precisely two thick edges, except those vertices sitting at the corners of the L_1 tiles (and vertices on the patch boundary, which are not important when we take the thermodynamic limit since we deal only with finite subgraphs interior to the region). We call each of these edges an e_0 edge. The corner vertices of L_1 tiles are exactly the 8-vertices of L_0 (this follows from the fact that every vertex becomes an 8-vertex under at most two inflations). Therefore this choice causes every vertex of AB* at L_0 to be met by two e_0 edges. Since every vertex meets precisely two edges, the sets of edges must form closed loops [84]. Therefore these loops constitute a set of FPLs on AB* as required.

While it is possible to find other sets of edges with these properties, we designate this choice the canonical one. With it, all closed loops respect the D_8 local symmetry of AB and AB*.

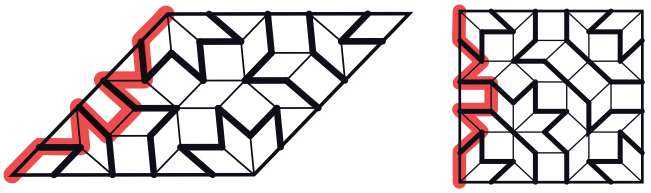

FIG. 3. Twice inflations of each of the two AB prototiles. We denote the smaller tiles composition-level zero L_0 and the larger tiles L_1. The thick black edges visit all but the corner vertices. We call these edges e_0 edges. Since the 8-vertices at L_0 corresponds to the tile vertices at L_1, the union of e_0 constitutes fully packed loops on AB* (AB without the 8-vertices). Augmenting the red path (switching covered and noncovered edges) places loop ends on the two corner vertices while still visiting the original vertices. The red path can be thought of as the twice inflation of an L_1 edge, and we term it e_1. It has the same effect along any tile edge. Augmenting cycles built from e_1 then places all visited 8-vertices onto the same loop.

B. Constructing fully packed loops and Hamiltonian cycles on AB

We next seek to construct FPLs on AB rather than AB* by adding the missing 8-vertices onto the loops. In Fig. 3 we highlight in red an alternating path (with respect to e_0 edges) which connects nearest-neighbor vertices in L_1. Augmenting the red path (swapping which edges are covered by e_0 edges) has a number of effects. First, it places e_0 edges touching the two L_0 8-vertices on which the alternating path terminates. Second, it increases the total number of e_0 edges by one. Third, any vertex which was previously visited by a pair of e_0 edges is still visited by a pair of e_0 edges.

While other such paths are possible, this canonical choice has advantages when combined with the canonical choice of e_0 edges. First, it can be seen in Fig. 3 that exactly the same shape of path can be used on any edge of either L_1 tile to cause the set of three effects just listed. Second, it does so entirely within the tile itself, and so these augmentations can be carried out without reference to neighboring L_1 tiles. The augmentation can be undone by augmenting along the same path a second time, which turns out to be key.

The red alternating paths trace a route along L_0 graph edges which follows the L_1 edges as closely as possible while also alternating with reference to the e_0 edge placement. In a natural sense, then, the red path is the twice inflation of an edge of an L_1 tile. We therefore refer to the red path as an e_1 edge. In this way, e_0 edges connect $8_{n<0}$-vertices (i.e., any vertices *except* 8-vertices at L_0), while e_1 edges connect 8_0-vertices (8-vertices which can survive precisely zero deflations while remaining 8-vertices). Further inflations can be carried out by stitching e_1 edges together in exactly the same way that e_1 was formed from e_0. For example, e_2 edges, connecting 8_1-vertices, can be built from e_1 edges, and can equivalently be thought of as built from more e_0 edges. In general, 8_n-vertices can be connected by e_{n+1} edges. The first three levels are shown in Fig. 4.

In the limit $n \to \infty$, e_n is a fractal: Under $e_0 \to e_1$ the initial side length of any prototile is divided into nine segments each of length δ_S^{-2}. The same scaling occurs for all subsequent inflations, and so the box counting dimension of e_∞ is given as

$$\dim(e_\infty) = \lim_{n\to\infty} \frac{\log(9^n)}{\log(\delta_S^{2n})} = \frac{1}{\log_3(1+\sqrt{2})} \approx 1.246. \quad (2)$$

This fits with the intuition that the curve is space filling.

To complete the proof of the existence of an FPL on AB it remains to show that all 8-vertices can be placed onto closed e_n loops for sufficiently large n. The canonical edge covering places all $8_{n<0}$ vertices of AB onto e_0 loops. To add all 8_0-vertices onto loops, we place loops of e_1 edges according to the canonical edge placement. This placement was defined at level L_0, but note that the twice (de)composition of any AB tiling is another AB tiling. Therefore the placement is well defined at all levels.

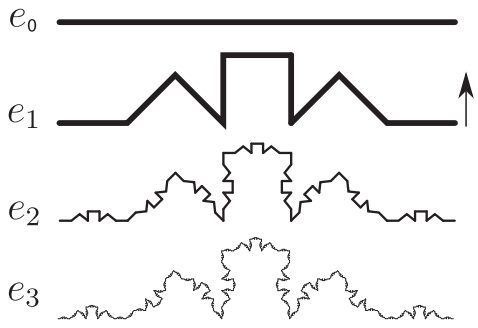

FIG. 4. The red alternating path in Fig. 3 can be thought of as a twice inflation of an e_0 edge from which loops are constructed at level zero (L_0). It connects nearest neighbors in the L_1 tiling (8-vertices in the L_0 tiling) while following an alternating path in the canonical choice of e_0 placements. We therefore denote this path an e_1 edge. Alternating paths connecting higher-order 8_n vertices can be constructed by concatenating e_{n+1} edges in the same way that e_1 was formed from a concatenation of e_0; levels e_2 and e_3 are shown here. We define the orientation of e_n according to the arrow.

Placing an e_1 edge means augmenting a path at L_0. Augmenting the closed loops of paths just defined places all 8_0-vertices visited by that loop onto loops of e_0 edges as required. We then proceed by induction, adding 8_n-vertices by connecting them with loops of e_{n+1} edges. After n steps, every vertex of order $8_{\leq n}$ is contained in a set of fully packed loops defined on those vertices. By design, placing the e_n edges does not cause problems with the existing matching of e_{n-1} edges. We refer the reader to Fig. 5 for an illustration of the e_1-loop structure (red), which clearly mirrors the smaller e_0-loop structure (black) constructed in Sec. III A.

While e_1 edges must follow the edges of L_1 tiles, two tiles meet along any edge. There is therefore a choice of two orientations of each e_1 owing to the choice of which of the two tiles e_1 lies within. Each e_1 orientation can be chosen freely with the statements in the previous paragraph remaining true. However, we find that there is again a natural choice. Define the orientation of e_1 to be in the direction indicated in Fig. 4. At L_1, we choose the sequence of e_1 edges along a loop to point alternately into then out of the loop on which it sits (this is implicit in the construction of e_2 and e_3 in Fig. 4). Since AB is bipartite, all loops are of even length, and there is never an inconsistency. When e_2 edges are placed, these will cut through e_1 loops. It is always possible to choose the orientations so that wherever e_1 loops and e_2 loops intersect, they do so along the length of one e_1 (recall that an e_2 is built from multiple e_1). Since these two e_1 overlap perfectly, augmenting them both has no overall effect at L_0. We can therefore delete both e_1. The effect is that the L_2 loops no longer intersect the L_1 loops: instead, they rewire separate L_1 loops so as to make them join together. Augmenting the L_1 star rewires all "cut" loops into one. By induction the rewiring works at all levels. The process is shown in detail in Appendix A, Figs. 11 and 12.

While it is already possible to reconnect many of these loops together, thereby building Hamiltonian cycles on subsets of the W_n vertices, the sets of vertices visited by such cycles always encircle sets of vertices they do not visit. To remedy this, it is necessary to break the D_8 symmetry. To see that this is necessary, consider the simplest D_8 Hamiltonian cycle, which is a star visiting the eight vertices adjacent to any 8-vertex, and the eight vertices immediately beyond them. To include the central 8-vertex on a loop, one of the points of the star must turn inward, breaking the symmetry.

In Fig. 5 we show a simple way to include the central region. The outermost e_n loop encircling the 8_n-vertex is the $2n$-fold inflation of the smallest star loop. By folding in a single corner of this inflated star, the loop now visits the central 8_n-vertex. In so doing, it connects *every* loop contained within it (and all those it passes through) into a single loop. The result is therefore a Hamiltonian cycle on the simply connected set of vertices visited by this deformed star. We denote this set U_n to distinguish it from the D_8-symmetric set W_n. The cycle on U_2 is shown in Fig. 6.

There is a topological reason this construction must work. Every closed e_0 loop bounds a D_8-symmetric region centered on an 8-vertex. Topologically we can imagine deforming the e_0 loops however we like, provided they cross neither 8-vertices nor other loops. Figure 3 shows that any path connecting two L_1 corners (8-vertices) along an L_1 edge must cross exactly four e_0 loops. One of these loops closes around one of the 8-vertices, while the three other loops close around the other 8-vertex (as well as other 8-vertices). This follows from Fig. 3, but a detailed proof appears in Appendix D of Ref. [39]. The situation is shown schematically in Fig. 7(a). Augmenting the red e_1 path along the L_1 edge rewires the L_0 loops according to Fig. 7(b). The same rewiring occurs for the blue edge in Fig. 7(c). While the augmentation illustrated in Fig. 7 leaves two string ends free, augmenting the closed L_1 star loop leads to a single closed loop at L_0. All subsequent levels of inflation L_n follow precisely the same pattern of connectivity. Having e_1 orientations (arrows in Fig. 7, defined in Fig. 4) point alternately in and out of the loop introduces a chirality that guarantees two facts. First, whenever an e_{n+1} loop cuts through e_n loops, the e_n loops merge. Second, the folded-corner outermost loop connects *all* loops within it. While this might at first seem miraculous, really it is no more complicated than the (folded) 16-vertex L_0 star hitting all 16 vertices in U_0: The U_n Hamiltonian cycle simply has n inflations (of both tiles and loops) applied according to the rules of Fig. 3.

C. Bounding the size of U_n

To see that any vertex set V must be contained within some U_n, recall linear repetitivity: Any V lying within a disk

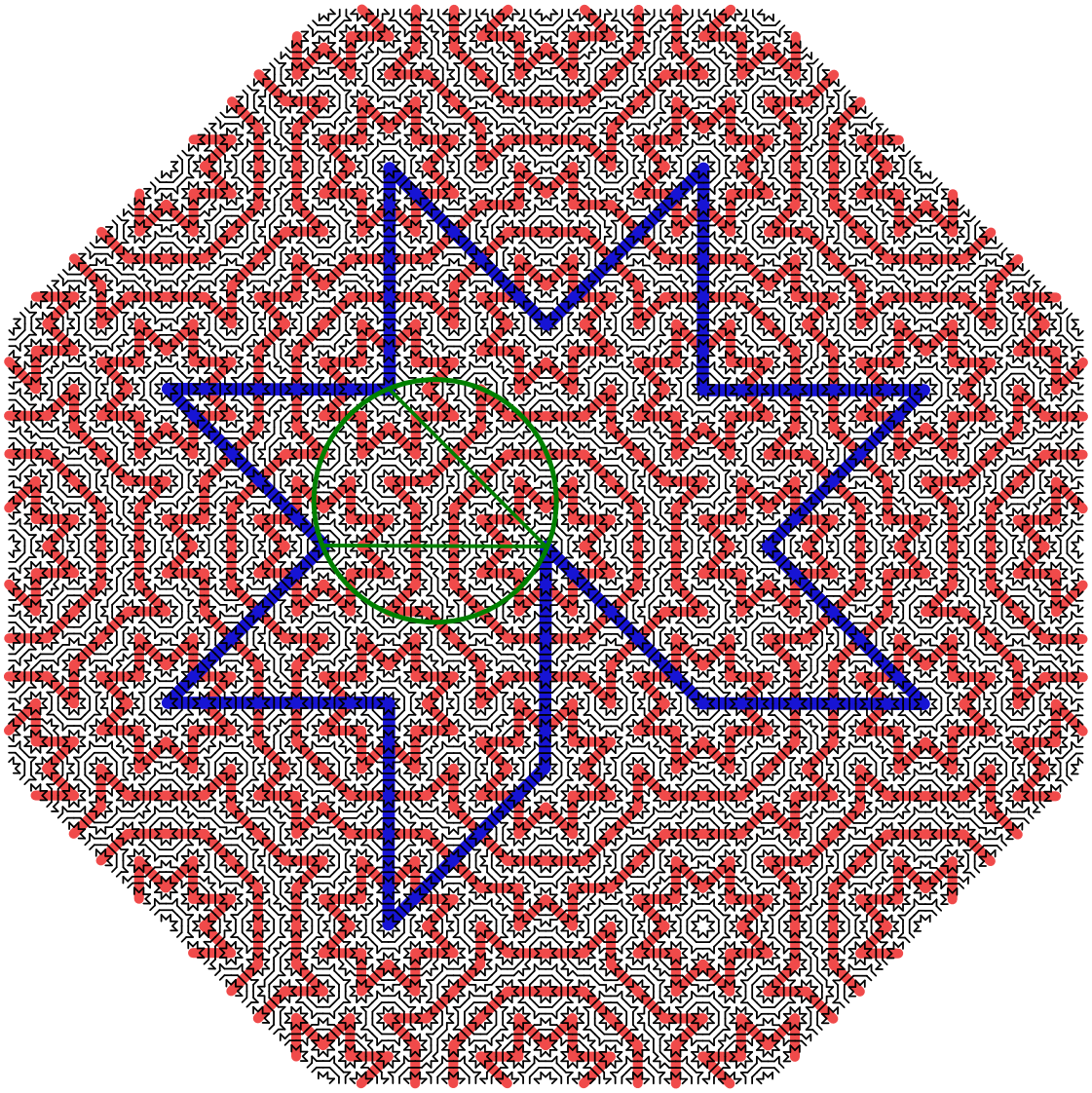

FIG. 5. The canonical placements of e_0 edges (black) form e_0 loops visiting every $8_{n<0}$-vertex (i.e., every vertex which is not an 8-vertex). The red lines form e_1 loops, along which e_1 edges from Fig. 4 can be placed adding all 8_0-vertices onto loops. Similarly, the blue star forms an e_2 loop, along which e_2 edges from Fig. 4 can be placed adding 8_1-vertices onto loops (see Fig. 11). The central 8-vertex is now added onto loops by folding one corner of the blue star inward to break the eightfold symmetry. Here we have shown the process explained in Sec. III B to order $n = 2$, but it can be iterated to any order n. In green is the largest disk fitting within the blue loop; the disk connects three 8-vertices with green chords.

of radius r must appear within *all* disks of radius Cr. Hence, any disk of radius Cr must contain all vertex configurations that can be contained within a disk of radius r.

Figure 5 shows a green disk contained within U_2. This is the largest disk fitting within the blue loop. Larger disks fit within U_2, but the boundary of successive U_n becomes fractal, whereas the equivalent to the blue loop maintains its shape at all levels of inflation, making the subsequent statements simpler. Denoting the green chord lengths l_2 (noting that these are edges of an L_2 rhombus) the radius of this disk is $2^{-1/4}\delta_S^{-1/2}l_2$. The largest equivalent disk in region U_n similarly has radius $2^{-1/4}\delta_S^{-1/2}l_n$. Denoting e_0 to be of unit length, the inflation rules of Fig. 2 imply that $l_n = \delta_S^{2n}$, and so U_n contains a disk of radius $2^{-1/4}\delta_S^{2n-1/2}$. Hence, linear repetitivity implies that every U_n contains every vertex set contained within a disk of radius $2^{-1/4}\delta_S^{2n-1/2}/C$. This radius grows exponentially and without bound in n, and so any V is contained within U_n for sufficiently large n (indeed, it is contained within all $U_{n\geq M}$ for sufficiently large M).

D. Thermodynamic limit

On any U_n we can construct a Hamiltonian cycle by the method outlined in Sec. III C. Since for any finite vertex set

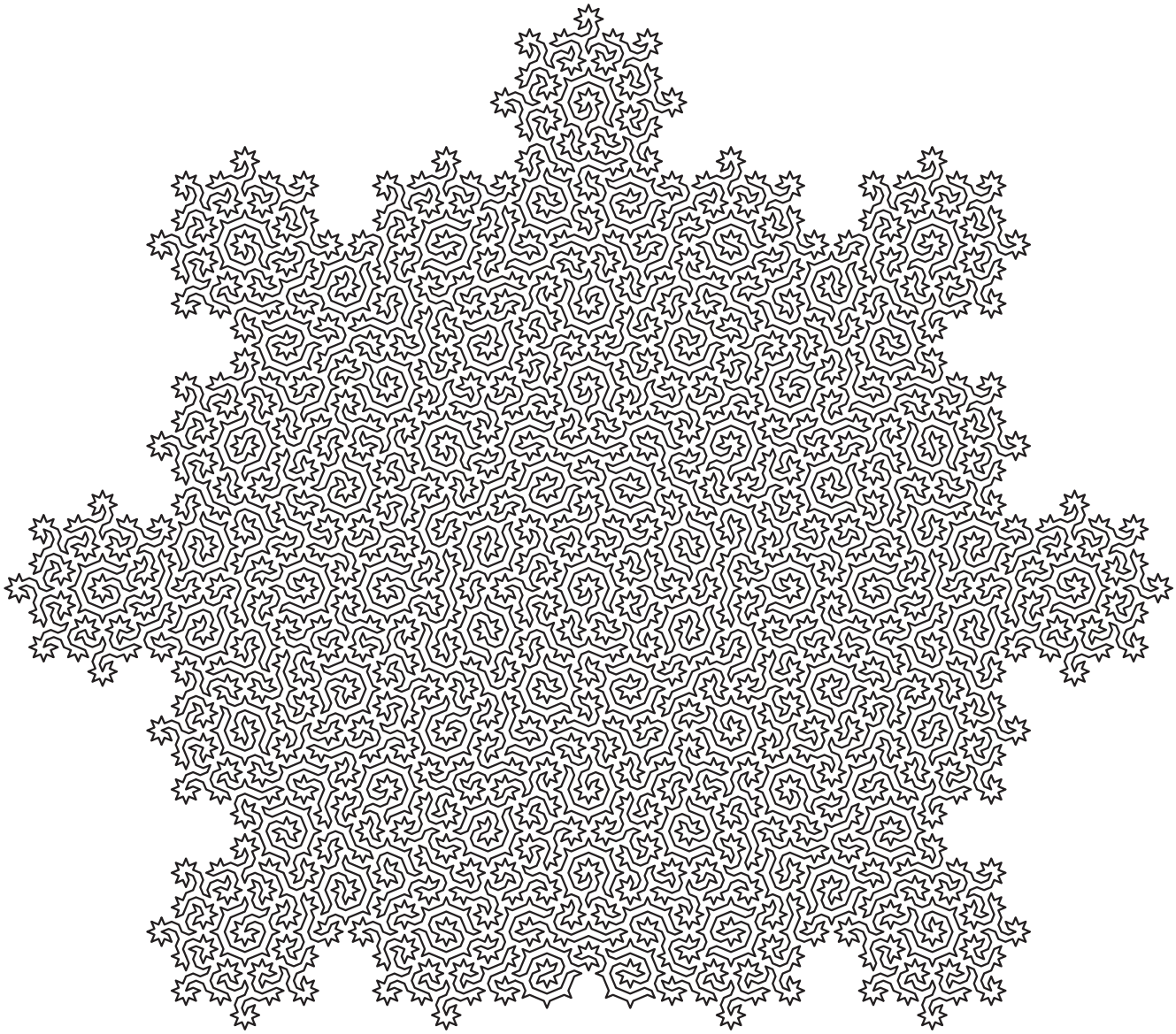

FIG. 6. The Hamiltonian cycle visiting all the vertices of a U_2 region (the AB tiles themselves are omitted for clarity). The image is obtained from Fig. 5 by placing e_1 and e_2 edges in alternate orientations along the red and blue loops, respectively, as shown in Fig. 11, and augmenting. Note the present figure has been rotated through $1/16$ of a turn relative to other figures to utilize the page efficiently.

V we can find a U_n such that $V \subseteq U_n$, the U_n admit a natural extension to the thermodynamic limit of macroscopically large cycles $U_{n\to\infty}$ (meaning arbitrarily large finite patches). The algorithm is of linear complexity in the number of vertices within U_n.

The region U_∞, without any surrounding tiles, can itself be thought of as an infinite AB tiling, in the sense that it is an infinite simply connected set of tiles generated by repeated inflations of a legitimate AB patch (followed by deletion of the surrounding tiles in W_∞).

It should be noted that an AB tiling can have at most one global center of D_8 symmetry (more than one would violate the crystallographic restriction theorem [85]), and the set of tilings with a global D_8 center is measure zero in the set of

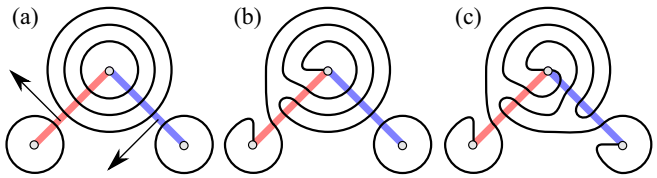

FIG. 7. The topology underlying the Hamiltonian cycle construction. (a) Every 8-vertex (gray disks) separated from another by an L_1 edge (red or blue) is enclosed by e_0 loops (black) as shown (see Fig. 3). Other 8-vertices are omitted for clarity. (b) [(c)] Augmenting the red [blue] e_1 edge, with e_1 orientation indicated with arrows as in Fig. 4, rewires the loops as shown. Hence, augmenting a *loop* of e_1 edges results in a *single* L_0 cycle visiting the chosen 8-vertices. The argument holds at all levels of inflation.

all possible AB tilings [77]. However, our definition of the thermodynamic limit does not rely on our tiling having a global D_8 center—it only needs to contain at least one $U_{n\to\infty}$, and all AB tilings contain infinitely many.

IV. SOLUTIONS TO OTHER NONTRIVIAL PROBLEMS ON AB

The question of whether an arbitrary graph admits a Hamiltonian cycle lies in the complexity class NPC. Problems in NPC are decision problems, meaning they are answered by either yes or no. The optimization version of these problems—to provide a solution if one exists—is instead typically in the class NP-hard (NPH). Finding a Hamiltonian cycle on an arbitrary graph is NPH.

In this section we provide exact solutions on AB for three problems made tractable due to discrete scale symmetry and/or by our construction of Hamiltonian cycles. In each case we state the decision problem and the corresponding optimization problem. Our choice of problems is motivated by the fact that on general graphs these decision problems lie in the complexity class NPC, and the corresponding optimization problems lie in the complexity class NPH. By solving the problems on AB we again show that this setting provides a special, simpler case.

A. Equal-weight traveling salesperson problem

Problem statement [63,86]. Given a number of cities N, unit distances between each pair of connected cities, and an integer k, does there exist a route shorter than k which visits every city exactly once and returns back to the original city? The corresponding optimization problem is to find such a route.

Solution on AB. If cities are the vertices of $U_{n\geq 0}$, yes if and only if $k > |U_n|$.

Proof. From a graph theory perspective, we can consider every city as a vertex and every direct route between a pair of cities as a weighted edge, where the associated weight denotes the distance between those cities. Finding the shortest route which can be taken by the traveling salesperson is equivalent to finding the lowest-weight Hamiltonian cycle, where the weight of the cycle is the sum of the weights of its edges. ∎

In this paper we have considered the unweighted AB graph, equivalent to setting all edge weights to one. In unweighted graphs the problem reduces to the equal-weight traveling salesperson problem. After this simplification, the unweighted decision problem becomes equivalent to the Hamiltonian cycle problem. Therefore the Hamiltonian cycle constructed in Sec. III solves the equal-weight traveling salesperson optimization problem on U_n.

1. Application: Scanning microscopy

One physical application of the traveling salesperson problem is to find the most efficient route to scan an atomically sized tip across a surface so as to visit every atom. For example, scanning tunneling microscopy involves applying a voltage between an atomically sharp tip and the surface of a material. Electrons tunnel across the gap between the tip and the sample, giving a current proportional to the local density of states in the material under the tip [87,88]. Magnetic force microscopy (MFM) uses a magnetic tip to detect the change in the magnetic field gradient [89,90]. The ultrahigh resolution nature of the imaging means that state-of-the-art measurements might take on the order of a month to scan a 100×100 nm^2 square region of a surface [91]. While generally applied to periodic crystalline surfaces, STM and MFM can in principle be used to image the surfaces of aperiodic quasicrystals, including those with the symmetries of AB tilings [44]. Unlike in the crystalline case, the most efficient route for the STM tip to visit each atom is not obvious in these cases. Our solution to the travelling salesperson problem optimization problem on AB provides a maximally efficient route for aperiodic quasicrystals with the symmetries of AB tilings. While the surface would need to be scanned once in order to establish the U_n regions to study, the purpose of STM and MFM would be to detect changes in the material under changing conditions (say, temperature or magnetic field), and the route provides maximum efficiency upon multiple scans.

B. Longest path problem

Problem statement [63,92]. Given an unweighted graph G and an integer k, does G contain a path of length at least k? We emphasize that the path may not revisit vertices. The corresponding optimization problem is to find a maximum length path.

Solution. Yes, if $G = U_{n\geq 0}$ and $k \leq |U_n| - 1$.

Proof. A Hamiltonian path can be obtained by removing any edge from a Hamiltonian cycle. The results of Sec. IV A imply that there exists a path of length $|U_n| - 1$ in any region U_n. ∎

Comment. Shorter paths can be found by deleting further contiguous edges. Since any AB tiling contains regions U_n, for any n, it follows that the tiling contains paths of any length.

1. Application: Adsorption

The "dimer model" in statistical physics seeks sets of edges on a graph such that each vertex connects to precisely one edge. It was originally motivated by understanding the statistics and densities of efficient packings of short linear molecules adsorbed onto the surfaces of crystals [93–95]. Noting again that certain physical quasicrystals have the

symmetries of AB tilings on the atomic scale, the existence of a longest path visiting every vertex shows that a long flexible molecule such as a polymer could wind so as to perfectly pack an appropriately chosen surface of such a material. The path can be broken into segments of any smaller length, showing that flexible molecules of arbitrary length can pack perfectly onto the surface. Dimers are returned as a special case.

Adsorption has major industrial applications. In catalysis, for example, reacting molecules can find a reaction pathway with a lower activation energy by first adsorbing onto a surface. While efficient packings can be identified on periodic crystals such as the square lattice, these feature a limited range of nearest-neighbor bond angles (with only right angles appearing in the square lattice). Realistic molecules, which have some degree of flexibility, might do better on quasicrystalline surfaces which necessarily contain a range of bond angles (four in AB). Other uses could include (hydro)carbon sequestration and storage, and protein adsorption [93,95].

C. Three-coloring problem

Problem statement [63,96]. Can all the faces of a planar graph G be colored such that no faces sharing an edge share a color? The corresponding optimization problem is to find such a three-coloring.

Solution. Yes, if $G \subseteq$ AB.

Proof. We know that the AB tiling is a bipartite graph which means that its vertices can be partitioned into two disjoint sets such that none of the edges has vertices belonging to the same set. We associate two opposite bipartite "charges" to the vertices depending upon which of these two mutually exclusive sets they belong to. ∎

We define two three-colored tiles, 1 and 2, as shown in Figs. 8(a) and 8(b), and repeat them over the entire tiling in the following manner.

(i) Place tile 1 over any 8-vertices having the same bipartite charge.
(ii) Place the mirror image of tile 1 over any 8-vertices having the opposite bipartite charge.
(iii) After that, place tile 2 or its mirror image such that the three rhombuses around every ladder, shown in Fig. 8(c), are the same color.

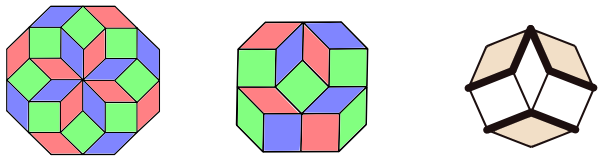

(a) Tile 1 (b) Tile 2 (c)

FIG. 8. (a),(b) Tiles used for three-coloring of the AB tiling. (c) The structure with three rhombuses present around every ladder.

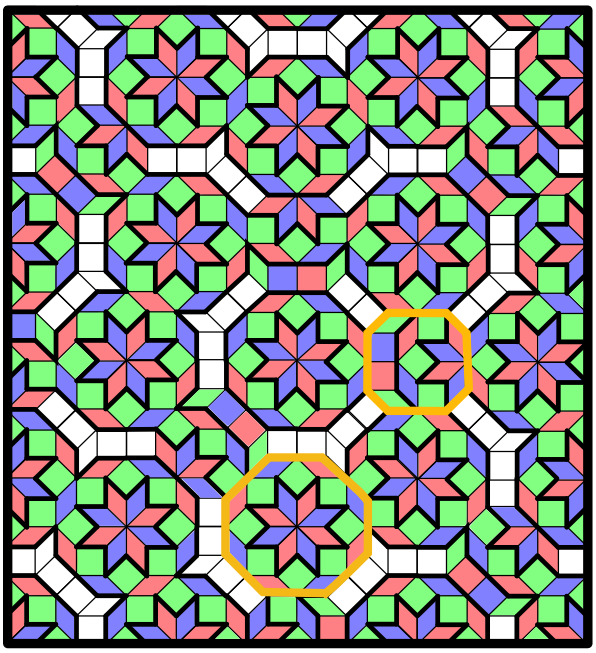

FIG. 9. A small patch of AB tiling three-colored using tile 1 and tile 2 (both outlined in gold) as mentioned in Sec. IV C. The only remaining portions of the tiling are segments of ladders which can be three-colored consistently on the basis of their surrounding tiles.

The consistent placement of these two tiles on the whole tiling is ensured by the structure of the tiling itself. After filling the whole AB tiling with these two tiles, all that remain are ladders, as shown in Fig. 9, which can be colored consistently on the basis of colors of their surrounding rhombuses such that no two adjacent faces should have a same color.

The three-coloring solution for the AB tiling is shown in Fig. 13. Note that the three-colorings are not unique.

Comments. This proof does not rely directly on the existence of Hamiltonian cycles. Rather, it relies on an intermediate step in their construction (specifically, the existence of fully packed loops on AB*; see Sec. III A), as well as the discrete scale invariance of AB. This proof demonstrates that the intermediate steps in our Hamiltonian cycle construction can already unblock problems that lie in the complexity class NP in general graphs, without necessarily needing to appeal to the finished result.

As an historical note, the five-coloring theorem, which states that any political map requires at most five colors in order to avoid any neighboring countries being the same color, was proven in the 19th century [97]. The equivalent four-coloring theorem was an infamous case of a problem which is easy to state but difficult to solve. The eventual proof in 1976 was the first major use of theorem-proving software, and no simple proof has been forthcoming [98]. The three-coloring problem is known to be NPC [63] on general graphs. However, special cases can again be

solved. A polynomial-time algorithm for generating a three-coloring of the rhombic Penrose tiling was deduced in 2000 [99], following its conjectured existence by Conway. The proof in fact covers all tilings of the plane by rhombuses, and therefore includes AB tilings. Our own solution to the three-coloring problem on AB tilings takes a different approach, and generates different three-colorings.

1. Application: The Potts model and protein folding

The q-state Potts model, $q \in \mathbb{N}$, is a generalization of the Ising model to spins σ_i which can take one of q values [69]. It is defined by the Hamiltonian,

$$H = -J\sum_{\langle ij\rangle}\delta_{\sigma_i,\sigma_j}, \tag{3}$$

where the sum is over nearest neighbors and δ is the Kronecker delta [69]. We can define the Potts model on the AB tiling by placing one spin on the center of each face of the tiling, with the four nearest neighbors defined to be the spins situated on the faces reached by crossing one edge.

The Potts model has a broad range of applications in statistical physics and beyond. It shows first and second order phase transitions, and infinite order BKT transitions, under different conditions of J and q. It is used to study the random cluster model [100], percolation problems [101], and the Tutte and chromatic polynomials [102]. Its physical applications include quark confinement [103], interfaces, grain growth, and foams [101], and morphogenesis in biological systems [104]. While most extensively studied on periodic lattices, there is some work on the Potts model in Penrose tilings; This model appears to show the universal behavior present in the periodic cases [105,106].

For $J > 0$, the model has a ferromagnetic ground state with all spins aligned along one of their q directions. The behavior for $J < 0$ is more complex. For $q = 2$, the model is the Ising model; since a two-coloring of the faces of AB is impossible (ruled out by the existence of three-vertices), the antiferromagnetic ground state must be geometrically frustrated, meaning the connectivity of sites causes spins to be unable to simultaneously minimize their energies.

However, the existence of a face-three-coloring proves that for $q \geq 3$ the $J < 0$ state is again unfrustrated. Three-colorings give the possible ground states of $q = 3$, and a subset of ground states for $q \geq 4$.

The relationship between the Potts model and the process of protein folding has been widely studied in the field of polymer physics and computational biology [75,76,107]. The q-state Potts model has been used to model the thermodynamics of protein folding [108]. In this scenario the lattice is thought of as a solvent in which the protein exists. A protein is a chain of amino acids [13]. When dissolved it may achieve a stable configuration, typically remarkably compact, which enables its biological functions [14]. The folding process depends on the pairwise interactions between amino acids, set by the interaction with the solvent [1,13,75]. If the interactions between similar amino acids are attractive, they cluster together to form a compact folded structure. If these interactions are repulsive, similar amino acids try to spread out over the solvent sites, resulting in a protein which is folded, but not compactly [76]. For modeling proteins, the Hamiltonian in Eq. (3) represents interacting amino acids $\{\sigma_i\}$. For $J < 0$ similar amino acids will have repulsive interactions in a solvent according to Eq. (3). For $J < 0$ and protein chains consisting of only three different types of amino acids (each corresponding to a color), our three-coloring of AB also predicts one of the stable, minimum energy configurations in which the protein can fold such that each of the three types of amino acid sits on the center of a tile of corresponding color.

It seems reasonable to suppose that folding of long protein chains might be better modeled by approximating the solvent with a quasicrystalline surface rather than a simple periodic lattice. This is because quasicrystals provide an aperiodic surface with range of bond angles, unlike regular lattices which have restricted freedom. For instance, square and hexagonal lattices have only one bond angle each (90° and 120°, respectively), and one vertex type, whereas AB has three bond angles of 45°, 90°, and 135°, and a wide range of different local environments branching out from seven vertex types. The eightfold rotational symmetry of patches of AB is of a higher degree than is possible in any crystal (six being the maximum degree permitted by crystallographic restriction), additionally making AB a closer approximation to the continuous rotational symmetry of space.

V. CONCLUSIONS

We provided exact solutions to a range of problems on aperiodic long-range ordered Ammann-Beenker tilings, with a further three problems solved in Appendix B. There are undoubtedly many more nontrivial problems like these which can be solved on AB tilings by taking advantage of its discrete scale invariance.

To our knowledge only one of the problems we solved was covered by an existing result: The three-color problem was covered by a solution to the three-color problem for Penrose tilings which applied to all tilings of rhombuses [99]. It is reasonable to ask whether this previously known result might similarly have been used to solve a range of other problems on AB, in the same way we exploited solutions to the Hamiltonian cycle problem. While we cannot rule this out, three-colorings do not obviously seem to provide an organizing principle for the tiling in the way that our hierarchically constructed loops do.

Our construction relies on the fact that AB tilings are long-range ordered, allowing exact results to be proven in contrast to random structures. It is natural to wonder whether any of our results apply more generally in other

quasicrystals. Deleting every second edge along a Hamiltonian cycle creates a perfect dimer matching (division of the vertices into unique neighboring pairs). The existence of such a matching on a graph is therefore a necessary condition for the existence of Hamiltonian cycles. It is not a sufficient condition, as there exist efficient methods, such as the polynomial-time Hopcroft-Karp algorithm, for finding perfect matchings [109]. Seeking quasicrystals which admit perfect matchings might be a good starting point for finding other quasicrystals which admit Hamiltonian cycles. As a preliminary check, using the Hopcroft-Karp algorithm we found the minimum densities of unmatched vertices on large finite patches of quasiperiodic tilings generated using the de Bruijn grid method, with rotational symmetries from sevenfold up to 20-fold [110]. We found finite densities in each case, suggesting AB may be unique among the de Bruijn tilings in admitting perfect matchings or Hamiltonian cycles [111]. On the other hand, a preliminary check of the recently discovered "Hat" [112] and "Spectre" [113] aperiodic monotiles (single tiles which tile only aperiodically) suggest that these also admit perfect dimer matchings, even if vertices are added so as to make the graphs bipartite; however, the structure of these matchings seems to indicate that a continuation to fully packed loops is not possible.

All of these examples consider the simplest case in which the vertices and edges of the graph are those of the corresponding tiling. Figure 10(a) shows a Penrose tiling (gray lines) decorated with graph vertices (gray disks) and edges (black) such that the graph admits fully packed loops (purple) by construction. Identical Penrose rhombuses are decorated identically, so that this graph has the full symmetry of the tiling. In Fig. 10(b) we have augmented the alternating cycle surrounding any red cross. The result is a cycle (red) visiting every vertex on any Penrose tile adjoining a cross. Hence, this is a Hamiltonian cycle on an appropriate subgraph. The construction (based on a dimer construction in Ref. [61]) closely mirrors that for AB tilings: establishing fully packed loops (in this case by construction), before connecting the loops together. Using similar approaches we might reasonably expect our results to generalize to a much broader class of structures.

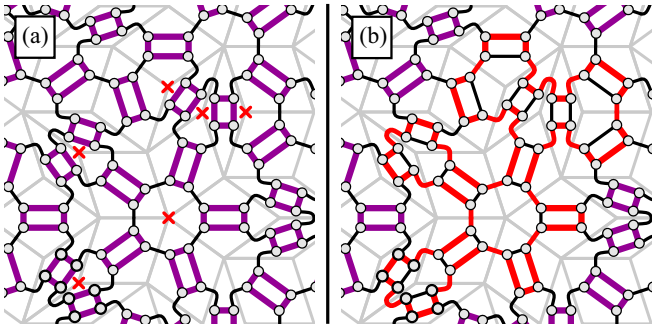

FIG. 10. (a) A Penrose tiling (gray lines) decorated by graph edges (black) and vertices (gray disks) so as to admit fully packed loops (purple) by construction. (b) Augmenting the alternating cycle surrounding each red cross leads to a cycle (red) which visits every graph vertex on any Penrose tile touching a cross.

Our Hamiltonian cycle construction included a proof of the existence of fully packed loops on arbitrarily large finite subgraphs of AB, in which every vertex is visited by a loop, but these need no longer be the same loop [114]. The FPL model is important for understanding the ground states of frustrated magnetic materials such as the spin ices [7]. Famously, loops played a key role in Onsager's exact solution to the Ising model in the square lattice, one of the most important results in statistical physics [115,116]. If all loops could be enumerated systematically, this would suggest the Ising model with spins defined on the faces of AB might be exactly solvable. We note that all possible dimer matchings were exactly enumerated on a modification of AB in which all the 8-vertices were removed, giving the partition function to the dimer problem [39]. The possible loop configurations can similarly be enumerated in that context.

There is a deep connection between loop and dimer models, and quantum electronic tight-binding models defined on the same graphs. For example, Lieb's theorem states that if a bipartite graph has an excess of vertices belonging to one bipartite sublattice, the corresponding tight-binding model must have at least the same number of localized electronic zero modes making up a zero-energy flat band [117]. These zero modes are topologically protected in the sense that they survive changes to the hopping strengths provided these strengths remain nonzero. Even if a bipartite graph has an overall balance of sublattice vertices, it can have locally defective regions in which zero modes are similarly localized [118]. This occurs, for example, in the rhombic P3 Penrose tiling, which has an overall balance between biparite sublattices, but local imbalances lead to a finite density of localized electronic zero modes in its tight-binding and Hubbard models [119–121], which can be exactly calculated using dimers [61]. Even if the bipartite sublattices balance *locally*, as in the AB tiling [39], it could still in principle be the case that the graph connectivity localizes electrons to certain regions. Recent work has identified such zero modes in the Hubbard model on AB [122]. Many, but not all, of these appear to fit a loop-based structure first identified in Penrose tilings [119] and subsequently more general graphs [123]. The same structures have recently been identified in the Hat aperiodic monotiles [124]. A deeper connection between the graph connectivities leading to electronic zero modes and the loops we identify here is an interesting avenue for further work.

Hamiltonian cycles and other loop models have been widely used for modeling protein folding, by approximating the molecules as living on the sites of a periodic

lattice [1,9,76]. This simplification has allowed the tools of statistical physics to be brought to bear on complex problems [1,15,16]. Quasicrystals may well serve as better models for such studies in which space is approximated with a discrete structure. Quasicrystals are able to feature higher degrees of rotational symmetry than crystals, providing a better approximation to the continuous rotational symmetry of real space [43]. They feature a wider range of nearest-neighbor bond angles, and the variety of structures at greater numbers of neighbors increases rapidly. Quasicrystals also lack discrete translational symmetry, a feature of lattices which could cause them to poorly approximate continuous space, although quasicrystals such as AB do feature a discrete scale invariance which might lead to similar shortcomings. Random graphs also have these benefits, but they lack the long-range order of quasicrystals required to obtain exact results such as those we have presented here.

In the context of NPC problems, exact solutions to Hamiltonian cycles are useful because they serve as benchmarking measures for new algorithms [125–127]. While the difficulty of NPC means no known algorithm is capable of deterministically solving all instances in polynomial time, several algorithms display a high success rate on many graphs [125,128,129]. Finding and classifying Hamiltonian cycle instances which prove "hard" for these algorithms has immediate practical applications and can provide key insight into the full NPC problem. A future goal would be to see how these modern Hamiltonian cycle algorithms perform when applied to AB regions admitting Hamiltonian cycles. Since AB sits at the borderline between regular and random graphs, it contains structures not present in either. Additionally, our Hamiltonian cycle construction is highly nonlocal, leveraging our understanding of the discrete scale symmetry of the tiling. Thus, it may prove a difficult test case: In that scenario, understanding which structures of AB prove hard for solvers would be a worthwhile challenge. We provided our U_1 and U_2 graphs to the developers of the state-of-the-art "snakes and ladders heuristic" (SLH) Hamiltonian cycle algorithm [125], who ran a preliminary test in this direction [130]. U_1 contains 464 vertices and U_2 contains 14 992 vertices. The SLH algorithm found a Hamiltonian cycle on U_1 in modest time ($\sim$1 s) but failed to find cycles on U_2 before exceeding the allotted memory. Given the large size of U_2, however, this is not conclusive evidence that AB is hard to solve. A next step would be a more thorough analysis, possibly identifying Hamiltonian cycle regions of more reasonable size for benchmarking purposes.

Another interesting direction might be to consider directed or weighted extensions of the graphs. Directed graphs can model non-Hermitian systems with gain and loss [131]; weighted graphs could model, for example, the traveling salesperson problem in which cities are connected by different distances. Finding a shortest route through a weighted graph is still an NPC problem, and the route would be selected from among the unweighted Hamiltonian cycles.

Our solution to the longest path problem shows that sets of flexible molecules of arbitrary lengths (not necessarily the same) can pack perfectly onto AB quasicrystals if they register to the atomic positions. This suggests applications to adsorption, which is relevant, for instance, to carbon capture [132] and catalysis: Two molecules might find a lower-energy route to reacting if they first bond to an appropriate surface before being released after reaction. Physical quasicrystals with three-dimensional point groups—"icosahedral" quasicrystals (iQCs)—are known to have properties which make them potentially advantageous as adsorbing substrates. Being brittle, they are readily broken into particles tens of nanometres in diameter, maximizing their surface area to volume ratio (a key consideration in industrial catalysis). They are stable at high temperatures, facilitating increased rates of reactions [133]. And, as discussed above, their surface atoms, lacking periodic arrangements, permit a wider range of bond angles. On the other hand, iQCs have been found to have high surface reactivities, which is unfavorable for catalysis because adsorbing molecules will tend to bond to the iQC substrate rather than to one another [134,135]. They also have low densities of states at the Fermi level compared to metals, which is unfavorable [53]. However, iQC nanoparticles have been successfully coated with atomic monolayers which then adopt their quasicrystallinity [136,137]; these monolayers include silver, a widely used and efficient catalyst with none of the quasicrystals' shortcomings [138]. Investigating the use of quasicrystals for such applications would therefore seem a profitable direction for future experiments.

The surfaces of iQCs have not been seen to feature the symmetries of AB; rather, they form a class of structures which includes Penrose tilings [134,135]. Further work is therefore needed to establish the possible packing densities of realistic iQC surfaces. Alternatively, the results presented here could potentially be put to use in the known two-dimensional "axial" quasicrystals which feature the symmetries of AB [44,45,139].

While AB tilings might have appeared to be an unlikely place to seek exact results to seemingly intractable problems, owing to their lack of periodicity, their long-range order makes such results obtainable. While periodic lattices feature a discrete translational symmetry which simplifies many problems (essentially enabling fields such as condensed matter physics, Floquet theory, and lattice QCD), quasicrystal lattices such as AB feature instead a discrete scale invariance. While less familiar, we would argue that this is just as powerful a simplifying factor. For example, the study of the electronic theory of solids is made possible by Bloch's theorem, which allows the electronic wave function to be calculated in infinite periodic lattices.

An equivalent to Bloch's theorem can be formulated for systems with discrete scale invariance [see, e.g., Eq. (1.4) in Ref. [140]], suggesting a comparable simplification in seemingly complex problems. To take another example, conformal theories, describing, for example, critical states at phase transitions, feature both continuous scale and continuous translation invariance. Our work opens the possibility of studying the breakdown of conformal symmetry into discrete scale invariance rather than the more familiar discrete translational invariance [50,141]. For example, we have established the possibility of studying fully packed loops on AB tilings; in periodic settings these admit conformal field theory descriptions [24]. The results presented here provide a key example of the simplifying power of discrete scale invariance.

Broadly, we might expect that many problems for which crystals are special cases might now find quasicrystals to also be special cases, albeit of a fundamentally different form.

ACKNOWLEDGMENTS

We thank J. C. Séamus Davis for providing estimates for scanning tunneling microscopy times, Francesco Zamponi for suggestions on Hamiltonian cycle benchmarking, Michael Haythorpe [125] for running the SLH Hamiltonian cycle finder algorithm on AB regions, Irene Giardina and Henna Koivusalo for helpful discussions, Michael Baake, Zohar Ringel, Steven H. Simon, Michael Sonner, and Jasper van Wezel for helpful comments on the manuscript, and Josh Colclough for the use of his code for generating de Bruijn grids. F. F. acknowledges support from EPSRC Grant No. EP/X012239/1.

APPENDIX A: DETAILED FIGURES

In this appendix we include detailed figures to accompany the proof sections in the main text. Figures 11 and 12 show intermediate steps for obtaining the Hamiltonian cycle in Fig. 6. In Fig. 11, black e_0 edges form loops visiting every $8_{n<0}$-vertex (i.e., every vertex which is not an 8-vertex). We placed red e_1 edges along the e_1 loops (red loops in Fig. 5) to add 8_0-vertices onto the loops. After this we also placed blue e_2 edges along the e_2 loop (blue loop in Fig. 5), with one corner folded, to add the central vertex and 8_1-vertices onto the loops. Note that some parts of the blue e_2 edges overlap with the red e_1 edges. Noting that augmentation of a set of edges is reversed by a second augmentation of the same set of edges, in Fig. 12 these overlapping e_2 edges and e_1 edges will augment to leave the L_0 tiling unchanged. Hence we can remove these overlapping edges completely. This results in a rewiring of e_1 loops and the e_2 loop into a single loop as shown. Augmenting this single loop, consisting of the remaining red and blue edges, will give us the Hamiltonian cycle shown in Fig. 6.

Figure 13 is a bigger version of Fig. 9, showing a solution for the three-coloring problem on a large patch of AB tiling resulting by placing tile 1 and tile 2 shown in Fig. 8, and coloring the remaining ladders consistently on the basis of colors of their surrounding rhombuses such that no two adjacent faces share a color.

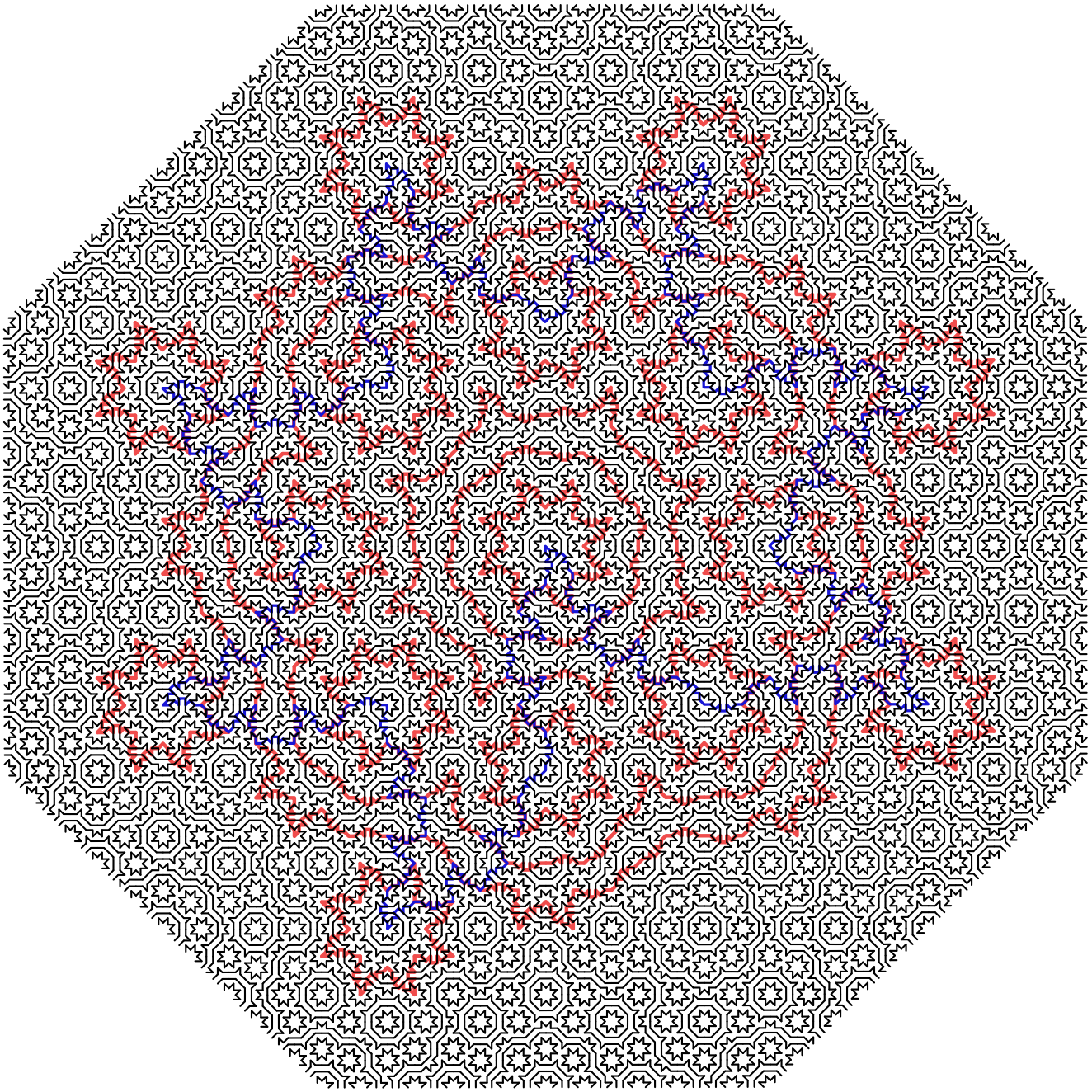

FIG. 11. The canonical placement of e_0 edges (black) forms loops visiting every $8_{n<0}$-vertex (i.e., every vertex which is not an 8-vertex). Now e_1 edges (red) are placed along the e_1 loops (see Fig. 5) to add 8_0-vertices onto the loops. Further e_2 edges (blue) are placed along the e_2 loop, with one corner folded, to add the central vertex and 8_1-vertices onto the loops. Note that some blue e_2 edges overlap with the red e_1 edges. This process can be iterated to any order.

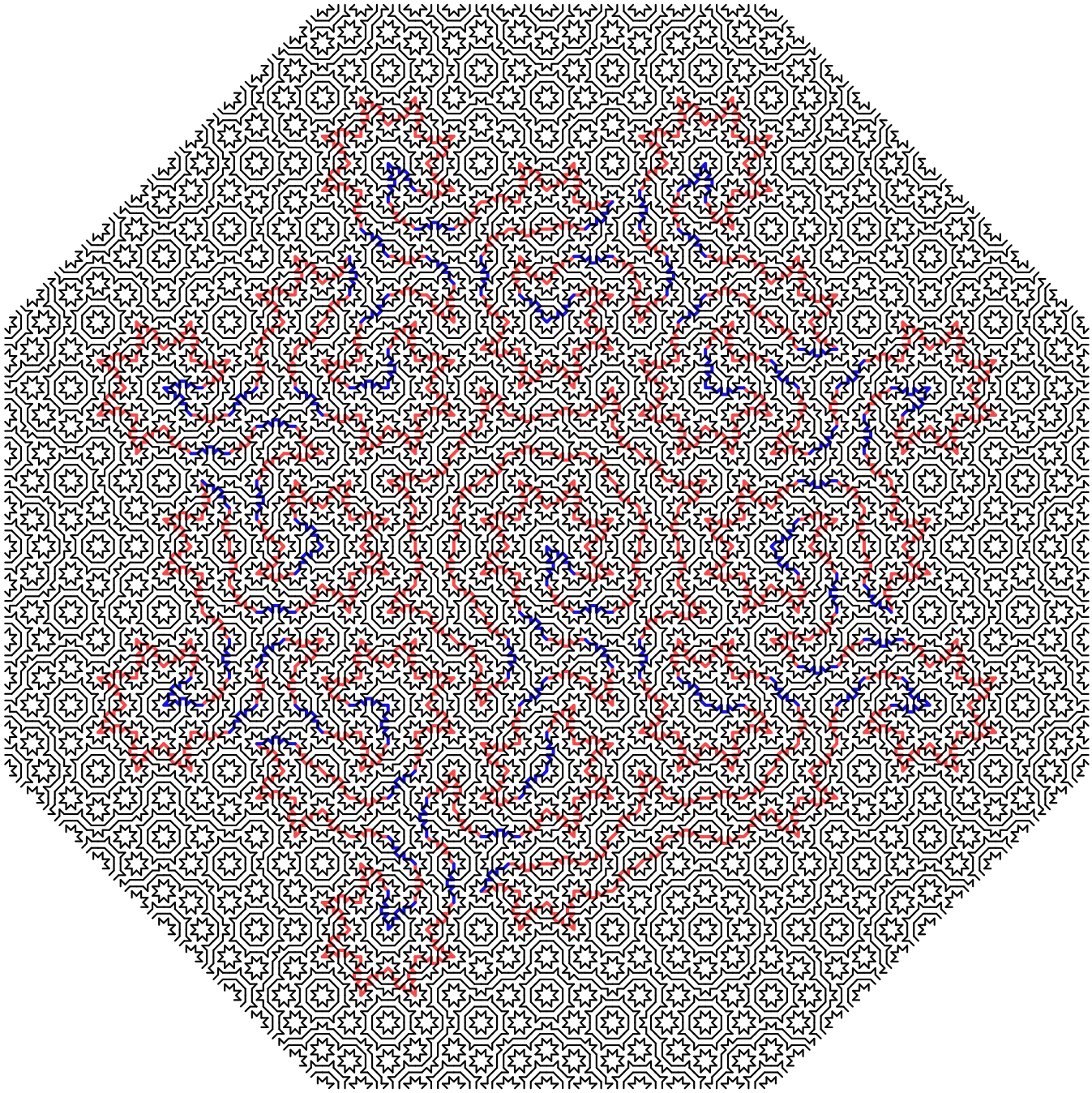

FIG. 12. The overlapping e_2 edges and e_1 edges as shown in Fig. 11 will augment to leave the L_0 tiling unchanged. Hence we can remove these overlapping e_2 edges and e_1 edges completely. This results in the rewiring of e_1 loops and the e_2 loop into a single loop as shown here. Finally augmenting this single loop, consisting of the remaining red and blue edges, will give the Hamiltonian cycle shown in Fig. 6.

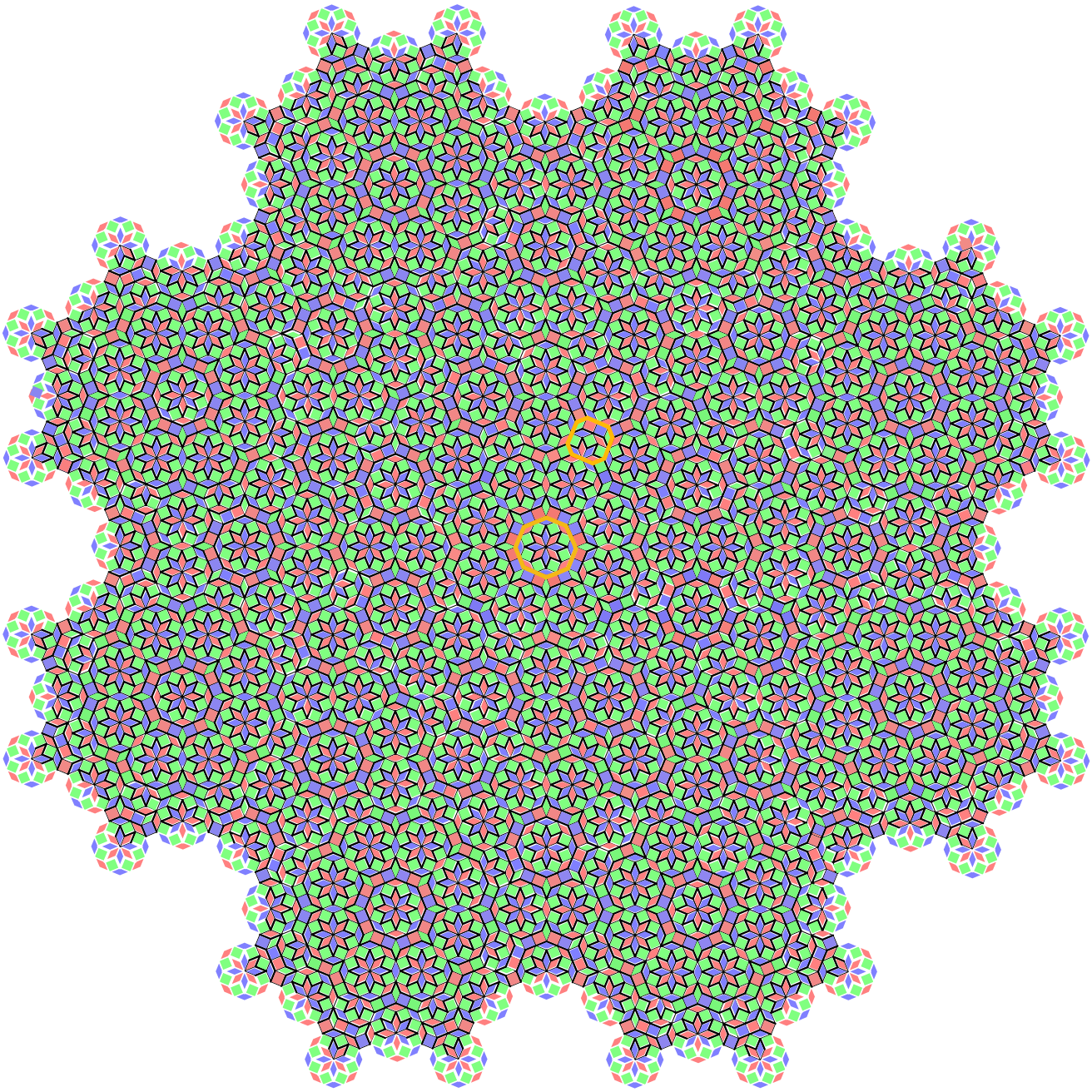

FIG. 13. The three-colored AB tiling using tile 1 and tile 2 (both outlined in gold) as mentioned in Sec. IV C.

APPENDIX B: SOLUTIONS TO OTHER NONTRIVIAL PROBLEMS ON AB

1. Minimum dominating set problem

A dominating set D of a graph G is a subset of the vertices of G such that all the vertices not in D are adjacent to at least one vertex in D. The minimum dominating set (MDS) is a dominating set containing the fewest possible vertices; its cardinality is called the domination number, $\gamma(G)$.

Problem statement [63]. Given a graph G and integer k, is the domination number $\gamma(G) \leq k$? The corresponding optimization problem is to find the MDS.

Solution. If G is built from N copies of $L_{1/2}$ tiles, yes if and only if $N \leq k$.

Proof. Figure 2 shows the single-inflation rules for the rhombus and square, level $L_{1/2}$. The set of red vertices forms an MDS for all vertices within each $L_{1/2}$ tile. Since these inflated tiles cover the entire tiling (owing to discrete scale symmetry), the union of minimum dominating sets of all these inflated tiles must be a dominating set for any patch of the AB tiling, or the tiling itself in the thermodynamic limit. That this is actually an MDS can be seen from the fact that there is no redundancy in the placement of the red vertices in Fig. 2: No red vertex has another red as

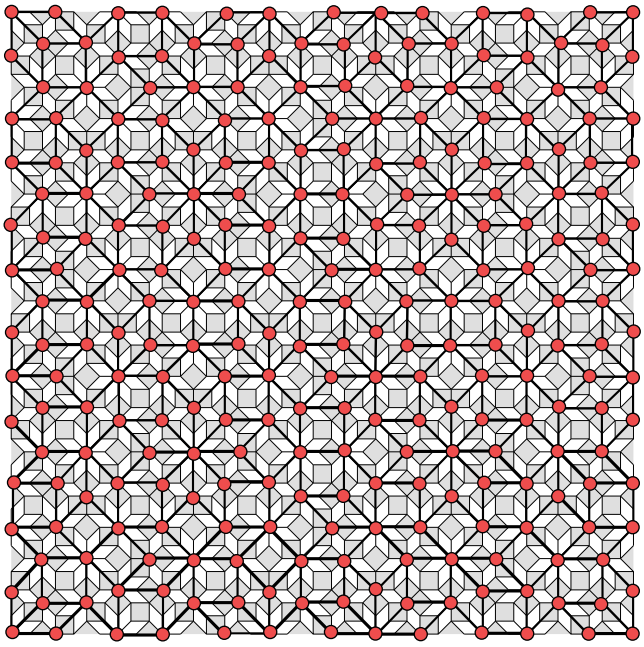

FIG. 14. A portion of AB tiling showing the minimum dominating set vertices (red), which as proved in Sec. B 1 are also vertices of single inflated tiles.

a neighbor, which implies that the set constitutes an MDS for the whole AB tiling. A larger region of the MDS is shown in Fig. 14. Note that the MDS is not unique. ∎

Comment. The proof relies only on the discrete scale symmetry of AB tilings, without reference to the Hamiltonian cycle construction.

2. Domatic number problem

The domatic number $d(G)$ for any given graph G with a set of vertices V is the maximum number of disjoint dominating sets into which V can be partitioned.

Problem statement [63,142]. For a given graph G and integer $3 \leq k \leq \delta(G)+1$, where $\delta(G)$ is the minimum degree of G, does G have a domatic number $d(G) \geq k$? The corresponding optimization problem is to find the corresponding dominating sets.

Solution. If $G = U_{n>0}$, yes if $k = 3$.

Proof. We will prove the result by using our Hamiltonian cycles to explicitly construct a partition of $U_{n>0}$ into three disjoint dominating sets. ∎

To see that the domatic number cannot be greater than $\delta+1$, consider the set $N(v)$ composed of a vertex v along with its δ neighbors, such that $|N(v)| = \delta+1$; then each dominating set D_i contains at least one vertex in $N(v)$, and each vertex in $N(v)$ is contained in at most one D_i. Thus $d \leq \delta+1$. The case $k = 2$ also trivially holds for any graph with no isolated vertices. Hence, finding $k = 3$ disjoint dominating sets is the first nontrivial instance of the problem, which is NPC on general graphs.

Before proving our statement for AB, we first anticipate the result by giving a simple proof that any Hamiltonian graph G of size $|G| = 3n$, for n integer, admits $k = 3$ disjoint dominating sets. We have not seen this statement made elsewhere. To see that it is true, we begin by labeling the three sets by the colors red, blue, and yellow, denoted R, B, Y. Starting from an arbitrary vertex v_1 of G, color v_1 red. Then, proceeding along the Hamiltonian cycle, color each vertex cyclically according to the three colors. Thus, v_2 is colored B, v_3 is colored Y, v_4 is colored R, and so on. The constraint $|V| = 3n$ ensures that the final vertex v_{3n}, neighboring v_0, is colored Y. In this way the cyclic structure of the coloring holds. Since (i) the Hamiltonian cycle visits every vertex and (ii) every vertex of a given color neighbors at least one vertex of each of the two remaining colors, we have constructed three disjoint dominating sets for $k = 3$.

The extension to the $G = U_{n>0}$ regions of AB, which we have proven admit Hamiltonian cycles, is similarly simple. The cyclic coloring along the Hamiltonian cycle proceeds exactly as above. However, we do not have $|U_n| = 3n$ (for example, $|U_1| = 464|$). Nevertheless, in Fig. 15 we show a suitable starting vertex of the Hamiltonian cycle (red star) such that the final vertex of the cycle (white star) neighbors one vertex of each color. The pictured section of the Hamiltonian cycle appears as the central region of the U_1 cycle shown in Fig. 1, and every Hamiltonian cycle

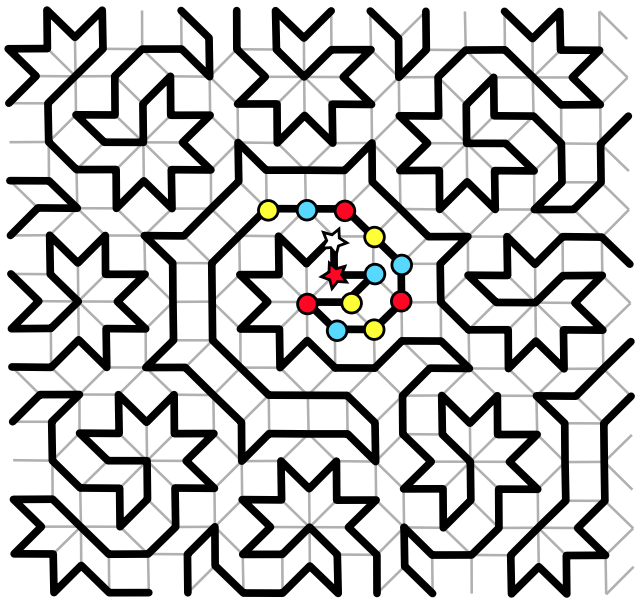

FIG. 15. Hamiltonian cycle structure (black edges), with vertices colored cyclically by the three colors R, B, Y, starting from the red star and proceeding clockwise around the cycle. The coloring scheme ensures that every vertex of a given color is neighbor to at least one vertex of each of the other colors; the final vertex in the cycle to be colored (white star) neighbors at least one vertex of each color, by construction. This proves that Hamiltonian subgraphs of AB have a domatic number $d \geq 3$.

constructed on $U_{n>0}$ according to our method follows an identical path at its center. Therefore, every vertex of a given color neighbors at least one vertex of each of the two remaining colors, and we have proven the case $k = 3$ for $U_{n>0}$. Note that U_0 is too small for this method to hold, and has $d = 2$.

Comments. Given that the minimum connectivity of AB is $\delta = 3$, the problem statement requests proof that the domatic number of $U_{n>0}$ is either $d = 3$ or $d = 4$. We have constructed a $d = 3$ partitioning using our Hamiltonian cycle construction. This solves the domatic number problem, which is NPC on general graphs.

The question of whether there exists a $d = 4$ partition remains open. We have been able to find such partitions of large regions of AB. We have not found any noticeable decrease in the freedom to continue the patterns as they grow. On the basis of these observations, we conjecture that a $d = 4$ partition is possible for arbitrarily large W_n regions. If true, this would render these arbitrarily large finite patches of AB tilings rare examples of "domatically full" graphs [143] with $d(G) = \delta(G) + 1$.

3. Induced path problem

An induced path in an undirected graph G is a sequence of vertices such that a pair of vertices is adjacent in the sequence if and only if the vertices have an edge in G. An induced cycle is an induced path which closes.

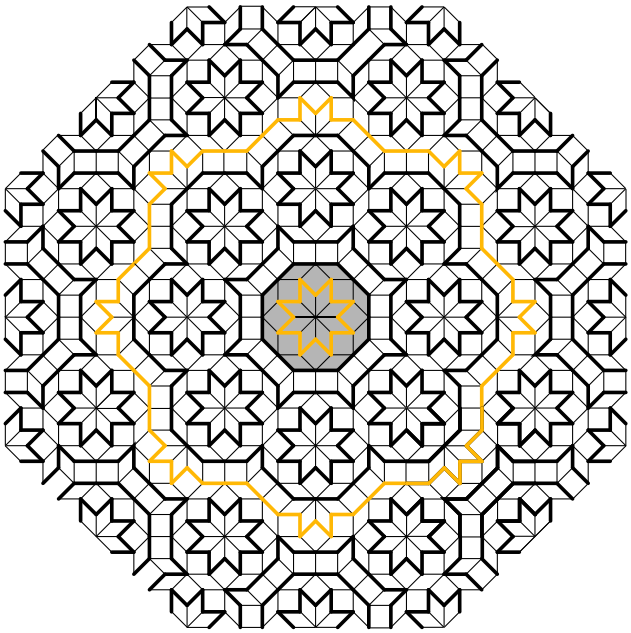

FIG. 16. FPLs on AB* formed by the method in Sec. III A form induced paths on AB. The longest induced path in region W_n created by this method is of length $8(9^n + 1)$. The total region shown here is W_1, with W_0 highlighted in gray. The corresponding induced paths are shown in gold.

Problem statement [63,144]. For a graph G and a positive integer k, does G contain an induced cycle of length at least k? The corresponding optimization problem is to find an induced cycle of length k.

Solution. Yes, if $G =$ AB.

Proof. In this case it is convenient to consider the D_8-symmetric regions W_n. Figure 16 shows the loops of the FPL on AB* constructed in Sec. III A. We see that any nonadjacent vertices on these loops do not have an edge in G, while any adjacent vertices do. Hence, these loops are induced cycles. The longest such loop in W_n is of length $8(9^n + 1)$ (this can be proven using the inflation rules of Fig. 2). Since any AB tiling contains W_∞, the answer to the problem is "yes" for any k, finite or infinite. ∎

Comments. On general graphs the problem remains NPC if an induced path is sought rather than an induced cycle. That problem can also be solved on AB, by deleting any pair of consecutive edges along the cycle. Longer induced cycles than those we consider can be found in W_n, but the problem statement does not require them.

[1] H. S. Chan and K. A. Dill, *Compact polymers*, Macromolecules **22**, 4559 (1989).

[2] P.-J. Flory, *Statistical thermodynamics of semi-flexible chain molecules*, Proc. R. Soc. A **234**, 60 (1956).

[3] H. Li, R. Helling, C. Tang, and N. Wingreen, *Emergence of preferred structures in a simple model of protein folding*, Science **273**, 666 (1996).

[4] H. E. Stanley, *Dependence of critical properties on dimensionality of spins*, Phys. Rev. Lett. **20**, 589 (1968).

[5] H. W. J. Blöte and B. Nienhuis, *Fully packed loop model on the honeycomb lattice*, Phys. Rev. Lett. **72**, 1372 (1994).

[6] R. J. Baxter, *Exactly Solved Models in Statistical Mechanics* (Academic Press, London, 1982).

[7] L. D. C. Jaubert, M. Haque, and R. Moessner, *Analysis of a fully packed loop model arising in a magnetic Coulomb phase*, Phys. Rev. Lett. **107**, 177202 (2011).

[8] J. d. Cloizeaux and G. Jannink, *Polymers in Solution: Their Modelling and Structure* (Oxford University Press, New York, 1991).

[9] O. Bodroza-Pantic, B. Pantic, I. Pantic, and M. Bodroza-Solarov, *Enumeration of Hamiltonian cycles in some grid graphs*, MATCH Commun. Math. Comput. Chem **70**, 181 (2013).

[10] G. Jannink, *Polymers in Solution: Their Modelling and Structure* (Clarendon Press, Oxford, 1990).

[11] B. Nienhuis, *Exact critical point and critical exponents of* O(n) *models in two dimensions*, Phys. Rev. Lett. **49**, 1062 (1982).

[12] J. L. Jacobsen and J. Kondev, *Conformal field theory of the Flory model of polymer melting*, Phys. Rev. E **69**, 066108 (2004).

[13] T. E. Creighton, *Protein folding*, Biochem. J. **270**, 1 (1990).

[14] K. A. Dill, S. Bromberg, K. Yue, H. S. Chan, K. M. Ftebig, D. P. Yee, and P. D. Thomas, *Principles of protein*

folding—a perspective from simple exact models, Protein Sci. **4**, 561 (1995).
[15] H. S. Chan and K. A. Dill, *Intrachain loops in polymers: Effects of excluded volume*, J. Chem. Phys. **90**, 492 (1989).
[16] K. F. Lau and K. A. Dill, *A lattice statistical mechanics model of the conformational and sequence spaces of proteins*, Macromolecules **22**, 3986 (1989).
[17] J. L. Jacobsen, *Exact enumeration of Hamiltonian circuits, walks and chains in two and three dimensions*, J. Phys. A **40**, 14667 (2007).
[18] R. Agarwala, S. Batzoglou, V. Dančík, S. E. Decatur, S. Hannenhalli, M. Farach, S. Muthukrishnan, and S. Skiena, *Local rules for protein folding on a triangular lattice and generalized hydrophobicity in the HP model*, J. Comput. Biol. **4**, 275 (1997).
[19] W. Orr, *Statistical treatment of polymer solutions at infinite dilution*, Trans. Faraday Soc. **43**, 12 (1947).
[20] M. N. Barber and B. W. Ninham, *Random and Restricted Walks: Theory and Applications*, Vol. 10 (CRC Press, Boca Raton, FL, 1970).
[21] P.-G. De Gennes, *Scaling Concepts in Polymer Physics* (Cornell University Press, Ithaca, NY, 1979).
[22] K. F. Freed, *Renormalization group theory of macromolecules*, J. Stat. Phys. **52**, 521 (1988).
[23] J. L. Jacobsen, *On the universality of fully packed loop models*, J. Phys. A **32**, 5445 (1999).
[24] J. Kondev, *Liouville field theory of fluctuating loops*, Phys. Rev. Lett. **78**, 4320 (1997).
[25] M. T. Batchelor, J. Suzuki, and C. M. Yung, *Exact results for Hamiltonian walks from the solution of the fully packed loop model on the honeycomb lattice*, Phys. Rev. Lett. **73**, 2646 (1994).
[26] E. H. Lieb, *Exact solution of the problem of the entropy of two-dimensional ice*, Phys. Rev. Lett. **18**, 692 (1967).
[27] J. Suzuki, *Evaluation of the connectivity of Hamiltonian paths on regular lattices*, J. Phys. Soc. Jpn. **57**, 687 (1988).
[28] S. Higuchi, *Field theoretic approach to the counting problem of Hamiltonian cycles of graphs*, Phys. Rev. E **58**, 128 (1998).
[29] J. Kondev, J. de Gier, and B. Nienhuis, *Operator spectrum and exact exponents of the fully packed loop model*, J. Phys. A **29**, 6489 (1996).
[30] M. Batchelor, H. Blöte, B. Nienhuis, and C. Yung, *Critical behaviour of the fully packed loop model on the square lattice*, J. Phys. A **29**, L399 (1996).
[31] O. Bodroža-Pantić, H. Kwong, and M. Pantić, *Some new characterizations of Hamiltonian cycles in triangular grid graphs*, Discrete Appl. Math. **201**, 1 (2016).
[32] A. Kast, *Correlation length and average loop length of the fully packed loop model*, J. Phys. A **29**, 7041 (1996).
[33] H. Orland, C. Itzykson, and C. de Dominicis, *An evaluation of the number of Hamiltonian paths*, J. Phys. Lett. **46**, 353 (1985).
[34] J. L. Jacobsen and J. Kondev, *Field theory of compact polymers on the square lattice*, Nucl. Phys. **B532**, 635 (1998).
[35] J. Kondev and J. L. Jacobsen, *Conformational entropy of compact polymers*, Phys. Rev. Lett. **81**, 2922 (1998).
[36] T. Schmalz, G. Hite, and D. Klein, *Compact self-avoiding circuits on two-dimensional lattices*, J. Phys. A **17**, 445 (1984).
[37] M. Peto, T. Z. Sen, R. L. Jernigan, and A. Kloczkowski, *Generation and enumeration of compact conformations on the two-dimensional triangular and three-dimensional fcc lattices*, J. Chem. Phys. **127**, 07B612 (2007).
[38] A. V. Melkikh and D. K. Meijer, *On a generalized Levinthal's paradox: The role of long- and short-range interactions in complex bio-molecular reactions, including protein and dna folding*, Prog. Biophys. Molec. Biol. **132**, 57 (2018).
[39] J. Lloyd, S. Biswas, S. H. Simon, S. A. Parameswaran, and F. Flicker, *Statistical mechanics of dimers on quasiperiodic Ammann-Beenker tilings*, Phys. Rev. B **106**, 094202 (2022).
[40] B. Grünbaum and G. C. Shephard, *Tilings and Patterns* (W. H. Freeman and Company, New York, 1986).
[41] R. Ammann, B. Grünbaum, and G. C. Shephard, *Aperiodic tiles*, Discrete Comput. Geom. **8**, 1 (1992).
[42] M. Baake and U. Grimm, *Mathematical diffraction of aperiodic structures*, Chem. Soc. Rev. **41**, 6821 (2012).
[43] M. Senechal, *Quasicrystals and Geometry* (Cambridge University Press, Cambridge, England, 1995).
[44] N. Wang, H. Chen, and K. H. Kuo, *Two-dimensional quasicrystal with eightfold rotational symmetry*, Phys. Rev. Lett. **59**, 1010 (1987).
[45] N. Wang, K. K. Fung, and K. H. Kuo, *Symmetry study of the Mn-Si-Al octagonal quasicrystal by convergent beam electron diffraction*, Appl. Phys. Lett. **52**, 2120 (1988).
[46] A. Uri, S. C. de la Barrera, M. T. Randeria, D. Rodan-Legrain, T. Devakul, P. J. D. Crowley, N. Paul, K. Watanabe, T. Taniguchi, R. Lifshitz, L. Fu, R. C. Ashoori, and P. Jarillo-Herrero, *Superconductivity and strong interactions in a tunable moiré quasiperiodic crystal*, Nature (London) **620**, 762 (2023).
[47] K. Viebahn, M. Sbroscia, E. Carter, J.-C. Yu, and U. Schneider, *Matter-wave diffraction from a quasicrystalline optical lattice*, Phys. Rev. Lett. **122**, 110404 (2019).
[48] M. Sbroscia, K. Viebahn, E. Carter, J.-C. Yu, A. Gaunt, and U. Schneider, *Observing localization in a 2D quasicrystalline optical lattice*, Phys. Rev. Lett. **125**, 200604 (2020).
[49] G. M. Sommers, M. J. Gullans, and D. A. Huse, *Self-dual quasiperiodic percolation*, Phys. Rev. E **107**, 024137 (2023).
[50] D. E. Gökmen, S. Biswas, S. D. Huber, Z. Ringel, F. Flicker, and M. Koch-Janusz, *Machine learning assisted discovery of exotic criticality in a planar quasicrystal*, arXiv:2301.11934.
[51] M. Ciardi, A. Angelone, F. Mezzacapo, and F. Cinti, *Quasicrystalline Bose glass in the absence of disorder and quasidisorder*, Phys. Rev. Lett. **131**, 173402 (2023).
[52] F. Flicker and J. van Wezel, *Quasiperiodicity and 2D topology in 1D charge-ordered materials*, Europhys. Lett. **111**, 37008 (2015).
[53] F. Flicker and J. van Wezel, *Natural 1D quasicrystals from incommensurate charge order*, Phys. Rev. Lett. **115**, 236401 (2015).

[54] Y. E. Kraus, Y. Lahini, Z. Ringel, M. Verbin, and O. Zilberberg, *Topological states and adiabatic pumping in quasicrystals*, Phys. Rev. Lett. **109**, 106402 (2012).
[55] K. A. Madsen, E. J. Bergholtz, and P. W. Brouwer, *Topological equivalence of crystal and quasicrystal band structures*, Phys. Rev. B **88**, 125118 (2013).
[56] M. Gardner, *Mathematical games: About the remarkable similarity between the Icosian game and the towers of Hanoi*, Sci. Am. **196**, 150 (1957).
[57] J. A. Bondy and V. Chvátal, *A method in graph theory*, Discrete Math. **15**, 111 (1976).
[58] R. W. Robinson and N. C. Wormald, *Almost all cubic graphs are Hamiltonian*, Random Struct. Algorithms **3**, 117 (1992).
[59] W. T. Tutte, *A theorem on planar graphs*, Trans. Am. Math. Soc. **82**, 99 (1956).
[60] L. Liu, G. P. T. Choi, and L. Mahadevan, *Quasicrystal kirigami*, Phys. Rev. Res. **4**, 033114 (2022).
[61] F. Flicker, S. H. Simon, and S. A. Parameswaran, *Classical dimers on Penrose tilings*, Phys. Rev. X **10**, 011005 (2020).
[62] R. M. Karp, *Reducibility among combinatorial problems*, in *Complexity of Computer Computations* (Springer, New York, 1972) pp. 85–103.
[63] M. R. Garey and D. S. Johnson, *Computers and Intractability: A Guide to the Theory of NP-Completeness* (W.H. Freeman and Company, New York, 1979).
[64] R. McGrath, J. Smerdon, H. Sharma, W. Theis, and J. Ledieu, *The surface science of quasicrystals*, J. Phys. Condens. Matter **22**, 084022 (2010).
[65] J.-M. Dubois, *New prospects from potential applications of quasicrystalline materials*, Mater. Sci. Eng. A **294–296**, 4 (2000).
[66] J. J. Kweon, H.-I. Kim, S.-h. Lee, J. Kim, and S. K. Lee, *Quantitative probing of hydrogen environments in quasicrystals by high-resolution NMR spectroscopy*, Acta Mater. **226**, 117657 (2022).
[67] R. Diehl, W. Setyawan, and S. Curtarolo, *Gas adsorption on quasicrystalline surfaces*, J. Phys. Condens. Matter **20**, 314007 (2008).
[68] R. J. Baxter, *Exactly Solved Models in Statistical Mechanics* (Elsevier, New York, 2016).
[69] F.-Y. Wu, *The Potts model*, Rev. Mod. Phys. **54**, 235 (1982).
[70] Y. Hattori, A. Niikura, A. P. Tsai, A. Inoue, T. Masumoto, K. Fukamichi, H. Aruga-Katori, and T. Goto, *Spin-glass behaviour of icosahedral Mg-Gd-Zn and Mg-Tb-Zn quasicrystals*, J. Phys. Condens. Matter **7**, 2313 (1995).
[71] Z. Islam, I. R. Fisher, J. Zarestky, P. C. Canfield, C. Stassis, and A. I. Goldman, *Reinvestigation of long-range magnetic ordering in icosahedral Tb-Mg-Zn*, Phys. Rev. B **57**, R11047 (1998).
[72] T. J. Sato, H. Takakura, A. P. Tsai, K. Shibata, K. Ohoyama, and K. H. Andersen, *Antiferromagnetic spin correlations in the Zn-Mg-Ho icosahedral quasicrystal*, Phys. Rev. B **61**, 476 (2000).
[73] A. Goldman, T. Kong, A. Kreyssig, A. Jesche, M. Ramazanoglu, K. W. Dennis, S. L. Bud'ko, and P. C. Canfield, *A family of binary magnetic icosahedral quasicrystals based on rare earths and cadmium*, Nat. Mater. **12**, 714 (2013).
[74] R. Tamura, A. Ishikawa, S. Suzuki, T. Kotajima, Y. Tanaka, T. Seki, N. Shibata, T. Yamada, T. Fujii, C.-W. Wang, M. Avdeev, K. Nawa, D. Okuyama, and T. J. Sato, *Experimental observation of long-range magnetic order in icosahedral quasicrystals*, J. Am. Chem. Soc. **143**, 19938 (2021).
[75] T. Garel and H. Orland, *Mean-field model for protein folding*, Europhys. Lett. **6**, 307 (1988).
[76] T. N. De Silva and V. Sivised, *A statistical mechanics perspective for protein folding from q-state Potts model*, arXiv:1709.04813.
[77] M. Baake and U. Grimm, *Aperiodic Order*, Vol. 1 (Cambridge University Press, Cambridge, England, 2013).
[78] Legal patches can be defined according to edge matching rules [77], and simply ensure that the starting patch corresponds to a group of tiles that can be found together within the infinite tiling. In practice, usually a single square or rhombus tile is used as the initial patch.
[79] A. Haynes, H. Koivusalo, and J. Walton, *A characterization of linearly repetitive cut and project sets*, Nonlinearity **31**, 515 (2018).
[80] F. Fang, S. Paduroiu, D. Hammock, and K. Irwin, *Non-local game of life in 2D quasicrystals*, Crystals **8**, 416 (2018).
[81] W. T. Tutte and W. T. Tutte, *Graph Theory*, Vol. 21 (Cambridge University Press, Cambridge, England, 2001).
[82] J. A. Bondy *et al.*, *Graph Theory with Applications*, Vol. 290 (Macmillan, London, 1976).
[83] G. Chartrand, *Introductory Graph Theory* (Courier Corporation, Boston, 1977).
[84] Strictly, loops can be open if they connect two points on the boundary. However, these open paths lie entirely in the region $W_n \backslash U_n$ so are not relevant to our construction on U_n.
[85] N. W. Ashcroft and N. D. Mermin, *Solid State Physics* (Harcourt College Publishers, New York, 1976).
[86] D. B. Shmoys, J. Lenstra, A. R. Kan, and E. L. Lawler, *The Traveling Salesman Problem*, Vol. 12 (John Wiley & Sons, Incorporated, New York, 1985).
[87] G. Binnig and H. Rohrer, *Scanning tunneling microscopy*, Surf. Sci. **126**, 236 (1983).
[88] P. K. Hansma and J. Tersoff, *Scanning tunneling microscopy*, J. Appl. Phys. **61**, R1 (1987).
[89] Y. Martin and H. K. Wickramasinghe, *Magnetic imaging by "force microscopy" with 1000 Å resolution*, Appl. Phys. Lett. **50**, 1455 (1987).
[90] U. Hartmann, *Magnetic force microscopy*, Annu. Rev. Mater. Sci. **29**, 53 (1999).
[91] State-of-the-art STM measurements can obtain intraunit-cell data on crystal surfaces; for a 100×100 nm^2 region this would exceed 250 000 pixels. A typical measurement takes around 100 ms, so if each pixel is scanned at 100 energies, the result takes around 29 days.
[92] D. Karger, R. Motwani, and G. D. Ramkumar, *On approximating the longest path in a graph*, Algorithmica **18**, 82 (1997).
[93] J. K. Roberts, *Some properties of adsorbed films of oxygen on tungsten*, Proc. R. Soc. A **152**, 464 (1935).
[94] R. Fowler and G. Rushbrooke, *An attempt to extend the statistical theory of perfect solutions*, Trans. Faraday Soc. **33**, 1272 (1937).

[95] O. J. Heilmann and E. H. Lieb, *Theory of monomer-dimer systems*, Commun. Math. Phys. **25**, 190 (1972).

[96] M. R. Garey, D. S. Johnson, and L. Stockmeyer, *Some simplified NP-complete problems*, in *Proceedings of the Sixth Annual ACM Symposium on Theory of Computing* (Association for Computing Machinery, New York, 1974), pp. 47–63.

[97] P. J. Heawood, *Map color theorems*, Quant. J. Math. **24**, 332 (1890).

[98] K. Appel and W. Haken, *Every planar map is four colorable*, Contemp. Math. **98**, xx (1989).

[99] T. Sibley and S. Wagon, *Rhombic Penrose tilings can be 3-colored*, Am. Math. Mon. **107**, 251 (2000).

[100] V. Beffara and H. Duminil-Copin, *The self-dual point of the two-dimensional random-cluster model is critical for $q \geq 1$*, Probab. Theory Relat. Fields **153**, 511 (2012).

[101] W. Selke and D. A. Huse, *Interfacial adsorption in planar Potts models*, Z. Phys. B **50**, 113 (1983).

[102] A. D. Sokal and B. Webb, *The multivariate Tutte polynomial (alias Potts model)*, Surveys Combinatorics **327**, 173 (2005).

[103] M. Alford, S. Chandrasekharan, J. Cox, and U.-J. Wiese, *Solution of the complex action problem in the Potts model for dense QCD*, Nucl. Phys. **B602**, 61 (2001).

[104] F. Graner and J. A. Glazier, *Simulation of biological cell sorting using a two-dimensional extended Potts model*, Phys. Rev. Lett. **69**, 2013 (1992).

[105] W. G. Wilson and C. A. Vause, *Evidence for universality of the Potts model on the two-dimensional Penrose lattice*, Phys. Lett. A **126**, 471 (1988).

[106] G. Xiong, Z.-H. Zhang, and D.-C. Tian, *Real-space renormalization group approach to the Potts model on the two-dimensional Penrose tiling*, Physica (Amsterdam) **265A**, 547 (1999).

[107] R. M. Levy, A. Haldane, and W. F. Flynn, *Potts Hamiltonian models of protein co-variation, free energy landscapes, and evolutionary fitness*, Curr. Opin. Struct. Biol. **43**, 55 (2017).

[108] R. B. Potts, *Some generalized order-disorder transformations*, in *Mathematical Proceedings of the Cambridge Philosophical Society* (Cambridge University Press, Cambridge, England, 1952), Vol. 48, pp. 106–109.

[109] J. E. Hopcroft and R. M. Karp, *An $n^{5/2}$ algorithm for maximum matchings in bipartite graphs*, SIAM J. Comput. **2**, 225 (1973).

[110] N. de Bruijn, *Algebraic theory of Penrose's non-periodic tilings of the plane I*, Indagationes Mathematicae (Proceedings) **84**, 39 (1981).

[111] J. Colclough, github.com/joshcol9232/tiling.

[112] D. Smith, J. S. Myers, C. S. Kaplan, and C. Goodman-Strauss, *An aperiodic monotile*, arXiv:2303.10798.

[113] D. Smith, J. S. Myers, C. S. Kaplan, and C. Goodman-Strauss, *A chiral aperiodic monotile*, arXiv:2305.17743.

[114] J. d. Gier, *Fully packed loop models on finite geometries*, in *Polygons, Polyominoes and Polycubes* (Springer, New York, 2009), pp. 317–346.

[115] L. Onsager, *Crystal statistics. I. A two-dimensional model with an order-disorder transition*, Phys. Rev. **65**, 117 (1944).

[116] R. P. Feynman, *Statistical Mechanics: A Set of Lectures* (CRC Press, Boca Raton, FL, 2018).

[117] E. H. Lieb, *Two theorems on the Hubbard model*, Phys. Rev. Lett. **62**, 1201 (1989).

[118] R. Bhola, S. Biswas, M. M. Islam, and K. Damle, *Dulmage-Mendelsohn percolation: Geometry of maximally packed dimer models and topologically protected zero modes on site-diluted bipartite lattices*, Phys. Rev. X **12**, 021058 (2022).

[119] M. Kohmoto and B. Sutherland, *Electronic states on a Penrose lattice*, Phys. Rev. Lett. **56**, 2740 (1986).

[120] A. Koga and H. Tsunetsugu, *Antiferromagnetic order in the Hubbard model on the Penrose lattice*, Phys. Rev. B **96**, 214402 (2017).

[121] E. Day-Roberts, R. M. Fernandes, and A. Kamenev, *Nature of protected zero-energy states in Penrose quasicrystals*, Phys. Rev. B **102**, 064210 (2020).

[122] A. Koga, *Superlattice structure in the antiferromagnetically ordered state in the Hubbard model on the Ammann-Beenker tiling*, Phys. Rev. B **102**, 115125 (2020).

[123] B. Sutherland, *Localization of electronic wave functions due to local topology*, Phys. Rev. B **34**, 5208 (1986).

[124] J. Schirmann, S. Franca, F. Flicker, and A. G. Grushin, *Physical properties of the hat aperiodic monotile: Graphene-like features, chirality and zero modes*, Phys. Rev. Lett. **132**, 086402 (2024).

[125] P. Baniasadi, V. Ejov, J. A. Filar, M. Haythorpe, and S. Rossomakhine, *Deterministic "snakes and ladders" heuristic for the Hamiltonian cycle problem*, Math. Program. Comput. **6**, 55 (2014).

[126] P. Baniasadi, V. Ejov, M. Haythorpe, and S. Rossomakhine, *A new benchmark set for traveling salesman problem and Hamiltonian cycle problem*, arXiv:1806.09285.

[127] J. Sleegers and D. van den Berg, *The hardest Hamiltonian cycle problem instances: the plateau of yes and the cliff of no*, SN Comput. Sci. **3**, 372 (2022).

[128] K. Helsgaun, *An effective implementation of the Lin-Kernighan traveling salesman heuristic*, Eur. J. Oper. Res. **126**, 106 (2000).

[129] D. L. Applegate, R. E. Bixby, V. Chvátal, and W. J. Cook, *The traveling salesman problem*, *The Traveling Salesman Problem* (Princeton University Press, Princeton, NJ, 2011).

[130] The SLH algorithm was run on an Intel Core i7-1165G7 machine with 4 cores, 2.80 GHz clock speed, and 32 GB RAM.

[131] F. L. Metz, I. Neri, and T. Rogers, *Spectral theory of sparse non-Hermitian random matrices*, J. Phys. A **52**, 434003 (2019).

[132] P. Webley and D. Danaci, *CO_2 capture by adsorption processes*, in *Carbon Capture and Storage*, RSC Energy and Environment Series No. 26, edited by M. Bui and N. Dowell (The Royal Society of Chemistry, London, 2020), pp. 106–167.

[133] D. Louzguine-Luzgin and A. Inoue, *Formation and properties of quasicrystals*, Annu. Rev. Mater. Res. **38**, 403 (2008).

[134] Z. Papadopolos, G. Kasner, J. Ledieu, E. J. Cox, N. V. Richardson, Q. Chen, R. D. Diehl, T. A. Lograsso, A. R. Ross, and R. McGrath, *Bulk termination of the quasicrystalline fivefold surface of $Al_{70}Pd_{21}Mn_9$*, Phys. Rev. B **66**, 184207 (2002).

[135] Z. Papadopolos, P. Pleasants, G. Kasner, V. Fournée, C. J. Jenks, J. Ledieu, and R. McGrath, *Maximum density rule for bulk terminations of quasicrystals*, Phys. Rev. B **69**, 224201 (2004).

[136] R. McGrath, J. Ledieu, E. J. Cox, and R. D. Diehl, *Quasicrystal surfaces: structure and potential as templates*, J. Phys. Condens. Matter **14**, R119 (2002).

[137] R. McGrath, J. A. Smerdon, H. R. Sharma, W. Theis, and R. Ledieu, *The surface science of quasicrystals*, J. Phys. Condens. Matter **22**, 084022 (2010).

[138] M. Pagliaro, C. Della Pina, F. Mauriello, and R. Ciriminna, *Catalysis with silver: From complexes and nanoparticles to morals and single-atom catalysts*, Catal. Chem. **10**, 1343 (2020).

[139] D. A. Rabson, N. D. Mermin, D. S. Rokhsar, and D. C. Wright, *The space groups of axial crystals and quasicrystals*, Rev. Mod. Phys. **63**, 699 (1991).

[140] O. Ovdat and E. Akkermans, *Breaking of continuous scale invariance to discrete scale invariance: A universal quantum phase transition*, in *Fractal Geometry and Stochastics VI*, edited by Uta Freiberg, Ben Hambly, Michael Hinz, and Steffen Winter (Birkhäuser, Cham, 2021), p. 209.

[141] S. Biswas and S. A. Parameswaran, *Discrete scale invariant fixed point in a quasiperiodic classical dimer model*, arXiv:2302.07879.

[142] E. Cockayne and S. Hedetniemi, *Optimal domination in graphs*, IEEE Trans. Circuits Syst. **22**, 855 (1975).

[143] E. J. Cockayne and S. T. Hedetniemi, *Towards a theory of domination in graphs*, Networks **7**, 247 (1977).

[144] M. Yannakakis, *The node deletion problem for hereditary properties, Computer Science Laboratory*, Princeton University, Report No. TR-240, 1978.